De novo missense variants in phosphatidylinositol kinase PIP5KIγ underlie a neurodevelopmental syndrome associated with altered phosphoinositide signaling

Authors

Manuela Morleo, Rossella Venditti, Evangelos Theodorou, ..., Vincenzo Nigro, David A. Sweetser, Brunella Franco

Correspondence

morleo@tigem.it (M.M.), dsweetser@mgh.harvard.edu (D.A.S.)

We describe a neurodevelopmental disorder associated with *de novo* gain-of-function variants in PIP5KIγ kinase. The variants cause perturbed endosomal function resulting from increased production of phosphatidylinositol 4,5 bisphosphate and enhanced association of F-actin at endosomes. Moreover, mutant zebrafish larvae recapitulate the phenotypes observed in affected individuals from our cohort.

Morleo et al., 2023, The American Journal of Human Genetics *110*, 1–17
August 3, 2023

https://doi.org/10.1016/j.ajhg.2023.06.012

CellPress

Please cite this article in press as: Morleo et al., *De novo* missense variants in phosphatidylinositol kinase PIP5KIγ underlie a neurodevelopmental syndrome associated with al..., The American Journal of Human Genetics (2023), https://doi.org/10.1016/j.ajhg.2023.06.012

ARTICLE

De novo missense variants in phosphatidylinositol kinase PIP5KIγ underlie a neurodevelopmental syndrome associated with altered phosphoinositide signaling

Manuela Morleo,[1,2,25,*] Rossella Venditti,[1,3,25] Evangelos Theodorou,[4,25] Lauren C. Briere,[4] Marion Rosello,[5] Alfonsina Tirozzi,[2,6] Roberta Tammaro,[1] Nour Al-Badri,[5] Frances A. High,[7] Jiahai Shi,[8] Undiagnosed Diseases Network, Telethon Undiagnosed Diseases Program, Elena Putti,[5] Luigi Ferrante,[1] Viviana Cetrangolo,[1] Annalaura Torella,[1,2] Melissa A. Walker,[9] Romano Tenconi,[10] Maria Iascone,[11] Davide Mei,[12] Renzo Guerrini,[12] Jasper van der Smagt,[13] Hester Y. Kroes,[13] Koen L.I. van Gassen,[13] Muhammad Bilal,[14] Muhammad Umair,[15] Veronica Pingault,[16] Tania Attie-Bitach,[16] Jeannine Amiel,[16] Resham Ejaz,[17] Lance Rodan,[18,19] Marcella Zollino,[20] Pankaj B. Agrawal,[21,22] Filippo Del Bene,[5,26] Vincenzo Nigro,[1,2,26] David A. Sweetser,[4,26,*] and Brunella Franco[1,23,24,26]

Summary

Phosphoinositides (PIs) are membrane phospholipids produced through the local activity of PI kinases and phosphatases that selectively add or remove phosphate groups from the inositol head group. PIs control membrane composition and play key roles in many cellular processes including actin dynamics, endosomal trafficking, autophagy, and nuclear functions. Mutations in phosphatidylinositol 4,5 bisphosphate [PI(4,5)P2] phosphatases cause a broad spectrum of neurodevelopmental disorders such as Lowe and Joubert syndromes and congenital muscular dystrophy with cataracts and intellectual disability, which are thus associated with increased levels of PI(4,5)P2. Here, we describe a neurodevelopmental disorder associated with an increase in the production of PI(4,5)P2 and with PI-signaling dysfunction. We identified three *de novo* heterozygous missense variants in *PIP5K1C*, which encodes an isoform of the phosphatidylinositol 4-phosphate 5-kinase (PIP5KIγ), in nine unrelated children exhibiting intellectual disability, developmental delay, acquired microcephaly, seizures, visual abnormalities, and dysmorphic features. We provide evidence that the *PIP5K1C* variants result in an increase of the endosomal PI(4,5)P2 pool, giving rise to ectopic recruitment of filamentous actin at early endosomes (EEs) that in turn causes dysfunction in EE trafficking. In addition, we generated an *in vivo* zebrafish model that recapitulates the disorder we describe with developmental defects affecting the forebrain, including the eyes, as well as craniofacial abnormalities, further demonstrating the pathogenic effect of the *PIP5K1C* variants.

Introduction

Phosphoinositides (PIs) are cellular membrane lipids produced by selective phosphorylation of the inositol head group of phosphatidylinositol. The inositol head group is phosphorylated at the 3, 4, and 5 positions to produce three monophosphates, three bisphosphates, and a single trisphosphate. The addition or removal of phosphate groups from the inositol head group is mediated by phosphoinositide kinases and phosphatases, respectively, which are all well conserved during evolution.

PIs are important regulators of the composition of organelle membranes, where they exhibit a highly localized subcellular distribution.[1] In addition, PIs recruit a wide range

[1]Telethon Institute of Genetics and Medicine (TIGEM), Pozzuoli, Naples, Italy; [2]Department of Precision Medicine, University of Campania "Luigi Vanvitelli," Naples, Italy; [3]Department of Molecular Medicine and Medical Biotechnology, University of Naples "Federico II," Medical School, Naples, Italy; [4]Center for Genomic Medicine, Divisions of Pediatric Hematology/Oncology and Medical Genetics and Metabolism, Department of Pediatrics, Massachusetts General Hospital, Harvard Medical School, Boston, MA, USA; [5]Sorbonne Université, INSERM U968, CNRS UMR 7210, Institut de la Vision, Paris, France; [6]Department of Epidemiology and Prevention, IRCCS NEUROMED, Pozzilli, Italy; [7]Division of Medical Genetics & Metabolism, Massachusetts General Hospital for Children, Boston, MA 02114, USA; [8]Department of Biochemistry, Yong Loo Lin School of Medicine, National University of Singapore, Singapore, Singapore; [9]Department of Neurology, Division of Neurogenetics, Child Neurology, Massachusetts General Hospital, Boston, MA, USA; [10]Clinical Genetics Unit, Department of Women and Children's Health, University of Padova, Padova, Italy; [11]Medical Genetics, ASST Papa Giovanni XXIII, 24127 Bergamo, Italy; [12]Meyer Children's Hospital IRCCS, Neuroscience Department, Florence, Italy; [13]Department of Genetics, University Medical Center Utrecht, Utrecht, the Netherlands; [14]Department of Biochemistry, Faculty of Biological Sciences, Quaid-i-Azam University, Islamabad, Pakistan; [15]Medical Genomics Research Department, King Abdullah International Medical Research Center & King Saud Bin Abdulaziz University for Health Sciences, Ministry of National Guard Health Affairs, Riyadh, Saudi Arabia; [16]Service de Médecine Génomique des Maladies Rares, et Institut Imagine, Hôpital Necker-Enfants Malades, Paris, France; [17]Division of Genetics, Department of Pediatrics, McMaster Children's Hospital, Hamilton, ON, Canada; [18]Department of Neurology, Boston Children's Hospital, Boston, MA, USA; [19]Division of Genetics and Genomics, Department of Pediatrics, Boston Children's Hospital, Boston, MA, USA; [20]Institute of Medical Genetics, A. Gemelli School of Medicine, Catholic University of the Sacred Heart, Rome, Italy; [21]Divisions of Newborn Medicine, Boston Children's Hospital, Boston, MA, USA; [22]Genetics and Genomics, The Manton Center for Orphan Disease Research, Boston Children's Hospital, Harvard Medical School, Boston, MA, USA; [23]Scuola Superiore Meridionale (SSM, School of Advanced Studies), Genomics and Experimental Medicine Program, Naples, Italy; [24]Medical Genetics, Department of Translational Medicine, University of Naples "Federico II," Via Sergio Pansini, 80131 Naples, Italy
[25]These authors contributed equally
[26]Senior authors
*Correspondence: morleo@tigem.it (M.M.), dsweetser@mgh.harvard.edu (D.A.S.)
https://doi.org/10.1016/j.ajhg.2023.06.012.

of enzymes, ion channels, scaffolding proteins, trafficking regulators, and cytoskeletal motors to membranes, regulating their function and localization.[2] The heterogeneous distribution and rapid turnover of PIs contributes to their regulation of key cellular functions, including membrane trafficking, actin dynamics, endosomal trafficking, plasma membrane composition, autophagy, and nuclear functions.[1,3–7]

The PI phosphatidylinositol 4,5 bisphosphate ([PI(4,5)P2] plays an important role in many cellular signaling pathways and has been extensively studied.[8] It is localized mainly at the plasma membrane of cells, although smaller pools are found on the membranes of endosomes, autophagosomes, and lysosomes.[9] PI(4,5)P2 is generated by either the phosphorylation of phosphatidylinositol 5-phosphate (PI5P) at position 4 by the phosphatidylinositol 5-phosphate 4-kinase (PIP4K) or by the phosphorylation of phosphatidylinositol 4-phosphate (PI4P) at position 5 by phosphatidylinositol 4-phosphate 5-kinase (PIP5K). Cellular levels of PI4P are approximately ten times higher than PI5P levels, so it seems plausible that the major synthetic pathway for the formation of PI(4,5)P2 involves the activity of PIP5Ks. Three isoforms have been described for PIP5K: PIP5KIα, PIP5KIβ, and PIP5KIγ.[10]

The PIP5KIγ protein localizes to the plasma membrane, focal adhesions, and adherens junctions;[11,12] to endosomal and lysosomal compartments; and to the nucleus.[13,14] Among the signaling-mediated downstream processes, PIP5KIγ regulates actin assembly, focal adhesion dynamics, and the trafficking of several proteins to and from the plasma membrane.[11,12,15–18] It plays a key role in the brain, where it is expressed in the radial glia, neuroblasts, and differentiated neurons during cerebral cortex development.[19] PIP5KIγ is one of the major regulators maintaining appropriate levels of the synaptic pool of PI(4,5)P2,[20] and it is essential for synaptic transmission and synaptic vesicle trafficking.[20–22] Loss of PIP5KIγ is embryonically lethal in mice.[22]

Pathogenic variants in multiple proteins regulating PI(4,5)P2 levels have been implicated in recessive neurodevelopmental Mendelian disorders. For example, Lowe syndrome, also known as oculocerebrorenal syndrome (OCRL, MIM: 309000, X-linked recessive), caused by loss-of-function variants in *OCRL* (MIM: 300535), typically presents with congenital cataracts, renal tubular dysfunction, and intellectual disability.[23] Joubert syndrome 1 (JBTS1, MIM: 213300, autosomal recessive), due to loss-of-function variants in *INPP5E* (MIM: 613037), is characterized by cerebellar hypoplasia/aplasia, ataxia, motor delays, and breathing abnormalities.[24] Congenital muscular dystrophy with cataracts and intellectual disability (MDCCAID, MIM: 607875, autosomal recessive) is due to loss of function of *INPP5K* (MIM: 607875).[25,26] All three of these genes encode 5-phosphatases that dephosphorylate PI(4,5)P2 to generate PI4P,[27–29] and the loss of enzymatic activity in these disorders leads to increased levels of PI(4,5)P2 in Lowe[30,31] and Joubert[32] syndromes, and presumably also in MDCCAID, as a consequence of the decreased phosphatase activity.[25,26]

By contrast, lethal congenital contractural syndrome 3 (LCCS3, MIM: 611369, autosomal recessive), due to loss of function of PIP5KIγ kinase (*PIP5K1C*, MIM: 606102), is associated with reduced PI(4,5)P2 levels.[33] This disorder is characterized by severe joint contractures, muscle atrophy, and respiratory insufficiency.[33]

Here, we report nine individuals with three heterozygous *de novo* missense variants in *PIP5K1C*. These unrelated individuals share an overlapping phenotypic spectrum comprising intellectual disability, developmental delay, microcephaly, seizures, ocular abnormalities, and dysmorphic features. We demonstrate that these are gain-of-function variants, resulting in increased PI(4,5)P2 levels. We further verified the accumulation of PI(4,5)P2 in early endosomes (EEs) in fibroblasts from one of the affected individuals, which, in turn, resulted in enhanced recruitment of filamentous actin (F-actin) on the endosomal compartment. We also show that the association of F-actin with EEs affects endosomal functionality, as observed in fibroblasts from the affected individual. In addition, we generated mutant zebrafish larvae that recapitulate the phenotype observed in affected individuals with defects of the forebrain, including eye development, as well as craniofacial abnormalities, further supporting the pathogenicity of the variants. Collectively, our data provide compelling evidence that these three *PIP5K1C* missense variants result in an autosomal-dominant neurodevelopmental disorder associated with aberrant PI signaling.

Material and methods

Ascertainment and study approval

All families provided informed consent. Individuals 1 (I-1) and 4 (I-4) were ascertained through their participation in the Undiagnosed Diseases Network (UDN) study, which was approved by the National Institutes of Health Intramural Institutional Review Board (IRB). Individual 2 (I-2) was ascertained through the Telethon Undiagnosed Disease Program (TUDP). Individuals 3, 5, 6, 7, 8, and 9 (respectively I-3, I-5, I-6, I-7, I-8, I-9) were ascertained clinically. The various research and clinical teams were connected with web-based tools Matchmaker Exchange[34] and GeneMatcher.[35] The procedures followed were in accordance with the ethical standards of the responsible committee on human experimentation (institutional and national) for all individuals studied. The parents and/or legally authorized representatives of all affected individuals gave permission for their inclusion in this publication. Written consent for the publication of photos was obtained for I-1, I-2, I-4, I-5, I-6, I-7, and I-8.

Variant identification and classification

Molecular genetic analyses were performed in different research and clinical diagnostic centers. The details of these analyses are given in supplemental information. The *PIP5K1C* variants were identified with whole-exome sequencing for eight affected individuals and whole-genome sequencing for the remaining individual. Trio or quad sequencing was performed for all but I-3 and I-8,

who had proband-only exome sequencing. Variant filtering was done through locally developed pipelines, taking into account the quality of the variant calling, presence in population databases, predicted impact on the encoded protein, and segregation of the variants. Clinical information was collected via standardized clinical templates that were completed by collaborating clinicians.

PIP5K1C transcript GenBank: NM_012398.3 was used for variant nomenclature. Most relevant *in silico* impact predictions were also evaluated, such as combined annotation-dependent depletion (CADD) version 1.4,[36] Varsome,[37] PolyPhen-2,[38] and SIFT.[39] gnomAD was used to assess population frequency.[40]

Cell cultures and treatments

Fibroblasts from I-2 and two unrelated control individuals were cultured in Dulbecco's Modified Eagle Medium (DMEM; Gibco) supplemented with 10% fetal bovine serum (FBS), 1% L-glutamine, 1% antibiotics (penicillin/streptomycin), and 1% sodium pyruvate. Cells were allowed to grow at 37°C and 5% CO_2.

Immunofluorescence

Cells were grown on glass coverslips and treated as described above. They were fixed for 10 min in 4% paraformaldehyde (PFA) in PBS, washed three times with PBS, and permeabilized with 0.05% saponin, 0.5% BSA, 50 mM NH_4Cl, and 1X PBS (blocking buffer) for 45 min. Cells were incubated with the following primary antibodies at room temperature (RT) for 2 h: anti-early endosome antigen 1 (EEA1) 1:200 (Cell Signaling Technologies, 3288T), anti-LAMP1 1:200 (Abcam, Ab24170), and anti-FLAG (Sigma-Aldrich, F1804). Phalloidin was used to detect actin (1:300, Life Technologies, A12380). Cells were then washed three times with PBS and incubated with the appropriate secondary antibody conjugated to Alexa Fluor 488 or Alexa Fluor 568 (Invitrogen) for 1 h at RT. DNA was stained with Hoechst (Sigma-Aldrich, 33342). After three washings with PBS, slides were mounted on coverslips with Mowiol (Millipore).

Detection and quantification of intracellular PI(4,5P)2 and PI4P levels

Fibroblasts from individual I-2 were double-stained for PI4P and PI(4,5)P2 and for endosomal or lysosomal compartments using anti-PI4P (Echelon Biosciences, Z-P004), anti-PI(4,5)P2 (Echelon Biosciences, Z-P045), anti-EEA1, and anti-LAMP1 antibodies following the protocol of Hammond et al.[41] Briefly, cells were fixed with 2% PFA for 15 min at RT, washed three times in PBS supplemented with 50 mM NH_4Cl, and permeabilized by using digitonin (20 μM) for 5 min in buffer A (20 mM PIPES, pH 6.8, 137 mM NaCl, and 2.7 mM KCl). After three rinses in buffer A, cells were blocked for 45 min with blocking solution (buffer A supplemented with 5% [vol/vol] FBS and 50 mM NH_4Cl) and incubated with primary antibodies diluted in blocking solution for 1 h at RT. Cells were then washed with buffer A, incubated with fluorescence-conjugated secondary antibodies for 1 h, and finally postfixed for 5 min in 2% PFA. 10–15 fields (each containing 10–15 cells) were randomly sampled and imaged at the same microscope settings (laser power and detector amplification) and below pixel saturation. The mean intensity per cell was determined with the ImageJ software. For total PI4P- or PI(4,5)P2-level measurements, a mask on the whole cell was generated, and the mean fluorescence intensities of PI4P, PI(4,5)P2, EEA1, and LAMP1 were measured. For PI(4,5)P2-level assessment at endosomes, a mask using the endosomal marker EEA1 was generated for each cell, and the mean intensities of both PI(4,5)P2 and EEA1 were measured in those regions. After background subtraction, the PI(4,5)P2 values were normalized singularly with their own EEA1 values.

Confocal fluorescence microscopy, image processing, and fluorescence quantification

Cells were imaged with a Plan-Apochromat 40×, 63×, or 100×/1.4 oil objective on a Zeiss LSM700, Zeiss LSM800, or LSM880 confocal system equipped with an AiryScan module and controlled by the Zen blue software. The images used for quantification were acquired with the same parameters (i.e., digital gain, laser power, magnification) and processed with Fiji (ImageJ; National Institutes of Health) software. Specifically, to calculate the percentage of EEA1/phalloidin-positive structures, EEA1 spots were identified for each cell by using the "analyze particles" tool of Fiji software, and the fluorescence mean intensities of phalloidin for each particle were measured. The percentage of EEA/phalloidin double-positive particles was calculated individually for each cell. Brightness and contrast were adjusted with Adobe Photoshop, and figure panels were assembled with Adobe Illustrator. All of the experiments were performed at least three times, and representative images are shown. For analysis of immunofluorescence data, 50–90 cells were counted for each condition.

Transferrin trafficking assays

Control and I-2 fibroblasts were seeded at 80% density into 24-well plates and cultured overnight. Cells were serum-starved for 1 h at 37°C, and then they were washed twice in cold PBS with 1% BSA and incubated with 50 μg/mL Alexa-Fluor-546-Transferrin (Tf, Thermo Fisher) for 1 h at 37°C. After extensive washing with complete HEPES-buffered DMEM, the recycling of Tf was followed by incubating the cells in complete medium at 37°C for the indicated time. To measure the Tf binding, fibroblasts were serum-starved for 2 h, washed twice in cold PBS supplemented with 1% BSA, and 50 μg/mL Alexa-Fluor-546-Tf was added for 1 h at 4°C. For the binding, cells were fixed soon after the incubation period. To evaluate the internalization, cells were washed extensively with complete HEPES-buffered DMEM, and Tf was followed by incubating the cells in the presence of complete medium at 37°C for the indicated times. The cells were then acid washed (150 mM NaCl, 10 mM acetic acid, pH 3.5) before fixing.

To perform quantitative image analysis, 10 randomly chosen fields that included 8–10 cells each were scanned with a 40× oil-immersion objective with the same setting parameters (laser power and detector amplification) below pixel saturation. The mean intensity per cell was determined with Fiji software, and all pixel values above background levels were quantified. All of the experiments were repeated at least twice, and representative images are shown.

Zebrafish husbandry and embryo maintenance

Zebrafish (*Danio rerio*) were maintained at 28°C on a 14-h light/10-h dark cycle. Fish were housed in the animal facility of the laboratory in the Institut de la Vision (Paris, France), which was built according to the respective local animal welfare standards. All animal procedures were performed in accordance with French and European Union animal welfare guidelines with protocols approved by the ethics committee for animal experimentation of Sorbonne Université (APAFIS#21323–2019062416186982).

In vivo mRNA microinjections, imaging, and phenotyping

Molecular cloning

To generate the pCS2+_PIP5K1C-WT, pCS2+_PIP5K1C-c.436G>A (p.Glu146Lys), pCS2+_PIP5K1C-c.614A>G (p.Tyr205Cys), pCS2+_PIP5K1C-c.662A>G (p.Tyr221Cys), and pCS2+_PIP5K1C-c.757G>A (p.Asp253Asn) plasmids, NEBuilder HiFi DNA Assembly Cloning Kit (New England Biolabs, E5520S) was used, and the PCR fragments were inserted into the pCS2+ plasmid[22] linearized with the EcoRI restriction enzyme. The primer sequences used to amplify the inserts are available upon request. Variants are shown in the GenBank: NM_012398.3 transcript.

mRNA synthesis

To synthesize mRNAs *in vitro*, pCS2+_PIP5K1C-WT, pCS2+_PIP5K1C-p.Glu146Lys, pCS2+_PIP5K1C-p.Tyr205Cys, pCS2+_PIP5K1C-p.Tyr221Cys, pCS2+_GFP, and pCS2+_CBE4max-SpRY[42] plasmids were linearized with NotI restriction enzyme, and mRNAs were synthesized by *in vitro* transcription with the mMESSAGE mMACHINE Sp6 kit (Ambion, AM1340) with 1 μL of guanosine triphosphate (GTP) from the kit added to the mix. The final products were purified with the RNeasy kit (QIAGEN, 74104).

Micro-injections

For the injection of the different *PIP5K1C* mRNAs, one nanoliter of each mix was injected into the cell at one-cell-stage zebrafish embryos. To form the synthetic single-guide RNA (sgRNA) complex prior to injection, a mix of 2 μL of the Alt-R CRISPR-Cas9 CRISPR RNA (crRNA) (100 pmol/μL) and 2 μL of Alt-R CRISPR-Cas9 trans-activating CRISPR RNA (tracrRNA) (100 pmol/μL) from Integrated DNA Technologies was incubated at 95°C for 5 min, cooled down to RT, and then kept on ice. One nanoliter of another mix containing cytosine base editor (CBE) mRNA (600 ng/μL) and the synthetic sgRNA complex (43 pmol/μL) was then injected into the cell of one-cell-stage zebrafish embryos. The crRNA sequences used in this study are listed in supplemental information.

Whole-embryo DNA sequencing

For genomic DNA extraction, single or pooled embryos were digested for 1 h at 55°C in 10 μL per embryo of lysis buffer (10 mM Tris, pH 8.0, 10 mM NaCl, 10 mM ethylenediaminetetraacetic acid [EDTA], and 2% SDS) with proteinase K (0.17 mg/mL, Roche Diagnostics) and inactivated for 10 min at 95°C. To sequence and check for frequency of mutations, each target genomic locus was PCR amplified with Phusion High-Fidelity DNA polymerase (Thermo Fisher Scientific, F-530XL). Sanger sequencing of the PCR products was performed by Eurofins. Sequence analyses were performed with ApE software v2.0.53c, and quantification of the mutation rate was done with the editR 1.0.10 online software.[43] The primer sequences used to amplify the *pip5k1ca* and *pip5k1cb* loci are listed in supplemental information.

Alcian blue staining

The staining was performed by using an acid-free protocol.[44] 3 days post-fertilization (dpf), larvae were fixed in 100% ethanol overnight at 4°C and rehydrated in 50% ethanol diluted in PBS for 10 min at RT. Larvae were then transferred overnight at RT in staining solution containing 0.02% Alcian blue solution (Sigma Aldrich, A5268) and 40 mM $MgCl_2$ in 70% ethanol solution. Larvae were washed once with H_2O and bleached, without being covered, with 3% H_2O_2 (Sigma Aldrich, H1009) and 2% potassium hydroxide (KOH, VWR, 26668.296) for 20 min at RT. Clearing was achieved with sequential glycerol/KOH washes: (1) 20% glycerol/0.25% KOH for 3 h, (2) 50% glycerol/0.25% KOH for 3 h, and then in 50% glycerol/0.1% KOH, where the embryos were stored at 4°C until imaging. Measurements of the cartilage elements were determined at 3 dpf from ventral views of Alcian blue-stained larvae by using ImageJ/FIJI v.1.0.

Imaging

A Leica MZ10F microscope was used to image the whole zebrafish embryos.

Statistical analyses

All statistical analyses were performed in GraphPad Prism 7. When comparing two samples, two-tailed Wilcoxon-Mann-Whitney tests were used. ns = not significant, **$p < 0.01$, ***$p < 0.001$, ****$p < 0.0001$. Details of statistical analysis and exact values of numbers quantified in each experiment can be found in the figure legends. The two-tailed non-parametric Wilcoxon-Mann-Whitney t test was applied to determine significance of the base-editing efficiency and cartilage measures.

Results

De novo variants in *PIP5K1C* are associated with intellectual disability, developmental delay, microcephaly, epilepsy, and visual abnormalities

Nine unrelated affected individuals with *de novo* missense variants in *PIP5K1C* were identified. Six subjects are male, and three are female. They range in age from 3 to 15 years old. I-1 has the c.436G>A (p.Glu146Lys) variant; I-4, I-5, I-6, I-7, I-8, and I-9 have the c.662A>G (p.Tyr221Cys) variant (mosaic in I-5); and I-2 and I-3 have the c.614A>G (p.Tyr205Cys) variant (Figure 1).

While formal developmental assessments were not available for all individuals, all were described as having developmental delay ranging from moderate to profound. The majority were not able to walk independently and were non-verbal or only used a few words. I-5, whose *PIP5K1C* variant was mosaic, was the least-severely affected. Full-scale IQ was assessed at 52, 57, and 67 for I-2, I-3, and I-5, respectively. IQ assessment was not available for the remaining individuals, although I-1, I-4, I-6, I-7, I-8, and I-9's clinical profiles suggested severe intellectual disability. Hypotonia was noted in five of the nine individuals. Seven of the nine have epilepsy (severe epilepsy initially manifested as infantile spasms in I-4, I-7, and I-8). Seven individuals had acquired microcephaly. Brain magnetic resonance imaging (MRI) reports did not reveal any consistent findings between affected individuals. Consistent with this, combined neuroradiology review of brain MRI images from I-1, I-2, I-4, and I-5 revealed normal or inconsistent non-specific findings.

Visual impairment and/or ophthalmologic abnormalities were reported in eight affected individuals, including optic nerve abnormalities in two of them. I-4 and I-5 were reported to have had microphthalmia in infancy, but this finding was not confirmed later in life. Common craniofacial features include hypertelorism; upper lip prominence with or without midface prominence; micrognathia or a history of micrognathia; and large, arched

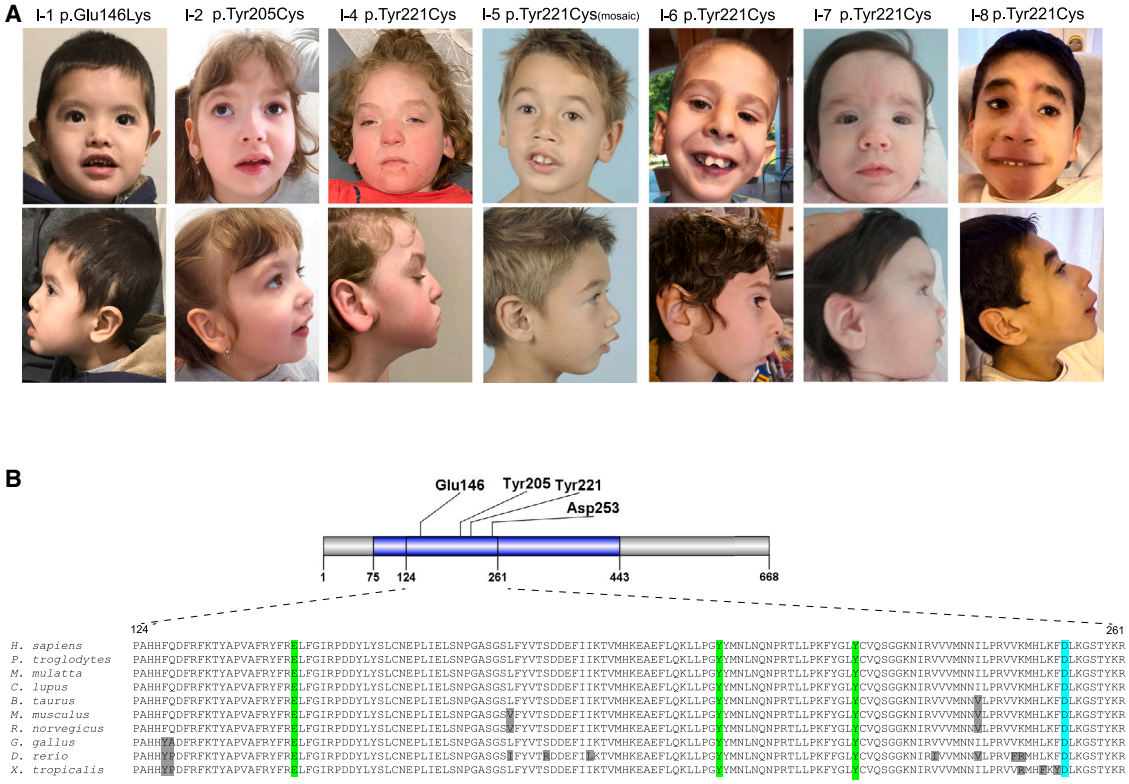

Figure 1. Clinical and genetic features of *PIP5K1C* neurodevelopmental syndrome

(A) Photos of I-1, I- 2, I-4, I-5, I-6, I-7, and I-8. Frequent facial features include prominent midface with protruding upper lip; broad nose with wide alae; hypertelorism; wide arched eyebrows; and ears that are long, posteriorly rotated, and have thickened superior helices. I-4 also has bilateral ptosis.

(B) Top: schematic illustration of the human PIP5KIγ protein showing the PIPK domain (blue) and the residues affected (Glu146, Tyr205, Tyr221) in our cohort and described by Narkis et al. (Asp253).[33] Bottom: amino acid sequence alignment for various PIP5KIγ vertebrate orthologs in the region of interest. Orthologs include *H. Sapiens* (NP_036530.1), *P. troglodytes* (XP_512274.3), *M. mulatta* (XP_002801072.1), *C. lupus* (XP_542172.5), *B. taurus* (NP_001009967.2), *M. musculus* (NP_032870.2), *R. norvegicus* (NP_001009967.2), *G. gallus* (XP_418191.4), *D. rerio* (XP_005171520.1 and XP_0051637202.1), and *X. tropicalis* (NP_001120474.1). Gray residues vary from the human reference. Green residues are those affected by the variants described here (Glu146, Tyr205, Tyr221), and the residue in light blue (Asp253) is the one described by Narkis et al.[33]

eyebrows. Concerns for abnormalities of the cranial sutures were raised in five of the nine individuals. I-2, I-4, and I-6 were noted to have prominent metopic ridges, I-1 had bilateral coronal synostosis, and a computed tomography (CT) scan in I-8 excluded craniosynostosis. Phenotype information of all affected individuals can be found in Table 1 and in the supplemental note. Details on *PIP5K1C* variants are reported in Table S1. Details on additional rare variants that segregated with the disease are reported in Table S2.

Protein structural analysis to assess pathogenicity of the germline *PIP5K1C* missense variants

We performed structural modeling of the p.Glu146Lys, p.Tyr205Cys, and p.Tyr221Cys variants, all of which are in the N terminus of the PIP5KIγ kinase domain (Figure S1). The variant p.Glu146Lys changes the surface charge from negative to positive (Figure S1) and likely affects the physical binding between PIP5KIγ and its interactors. The residues altered in the other two variants, p.Tyr205Cys and p.Tyr221Cys, form a cluster in the proximity of the ATP-binding motif of the PIP5KIγ kinase domain (Figure S1). These variants might reduce the side-chain volume of residues Tyr205 and Tyr221, enlarge the cavity of the ATP-binding pocket, and facilitate the binding of ATP at the pocket followed by enhancement of kinase activity.

Disease-associated *PIP5K1C* variants cause increased PI(4,5)P2 levels

To investigate whether the catalytic activity of PIP5KIγ is modified by the variants found in our cohort, we carried out detection and quantification of PI(4,5)P2 levels by immunofluorescence staining with a specific anti-PI(4,5)P2 antibody in I-2 and unrelated control fibroblasts. We observed a general increase of PI(4,5)P2 levels in I-2 fibroblasts (1.6-fold increase) compared with unrelated controls (Figure 2A), consistent with a gain-of-function effect of this variant.

Moreover, we noticed a higher number of PI(4,5)P2-positive intracellular spots in I-2-derived fibroblasts compared with control cells. Prompted by this

Please cite this article in press as: Morleo et al., *De novo* missense variants in phosphatidylinositol kinase PIP5K1γ underlie a neurodevelopmental syndrome associated with al..., The American Journal of Human Genetics (2023), https://doi.org/10.1016/j.ajhg.2023.06.012

Table 1. Variants in *PIP5K1C* cause a neurodevelopmental disorder, featuring intellectual disability, microcephaly, epilepsy, visual impairment, and/or ophthalmologic abnormalities

	I-1	I-2	I-3	I-4	I-5	I-6	I-7	I-8	I-9	Total
cDNA (GenBank: NM_012398.3)	c.436G>A	c.614A>G	c.614A>G	c.662A>G	c.662A>G[a]	c.662A>G	c.662A>G	c.662A>G	c.662A>G	–
Protein (GenBank: NP_036530.1)	p.Glu146Lys	p.Tyr205Cys	p.Tyr205Cys	p.Tyr221Cys	p.Tyr221Cys	p.Tyr221Cys	p.Tyr221Cys	p.Tyr221Cys	p.Tyr221Cys	–
Age at last evaluation	3 years	6 years	10 years	7 years	7 years	7 years	3 years	4 years	15 years	–
Motor delay	yes (walked at 5 years)	yes (walked at 30 months)	yes	yes (non-ambulatory)	yes (walked at 2 years)	yes	yes (non-ambulatory)	yes (non-ambulatory)	yes (non-ambulatory)	9/9
Speech delay	yes (nonverbal)	yes	yes (nonverbal)	yes (nonverbal)	yes	yes (nonverbal)	yes (nonverbal)	yes (nonverbal)	yes (nonverbal)	9/9
Intellectual disability	yes	yes	yes	yes	yes	yes	yes	yes	yes	9/9
Seizures	no	yes	yes	yes (DEE)	no	yes	yes (DEE)	yes (DEE)	yes	7/9
Visual impairment and/or ophthalmologic abnormalities	mild optic atrophy	-pale optic nerves -strabismus -myopia	mild myopia	-CVI strabismus -nystagmus -myopia -astigmatism	-probable CVI -mild hyperopia	-mild CVI -strabismus	-strabismus -astigmatism	no	strabismus	8/9
Hypotonia	yes	no	yes	yes	no	no	yes	yes	no	5/9
Brain MRI abnormalities	-abnormal lateral ventricles (contour) -abnormal white matter signal -Chiari malformation type 1 (s/p repair)	-abnormal white matter signal (delayed myelination) -focal dysgyria -agenesis of anterior falx cerebri	-abnormal white matter signal (hypomyelination)	-abnormal white matter signal (T2 prolongation) -possible focal dysgyria -cerebral atrophy	ND	ND	-abnormal lateral ventricles (microcysts in bilateral frontal horns)	-abnormal lateral ventricles (contour, septum pellucidum cyst) -focal dysgyria -velum interpositium cyst -increased CSF spaces at the temporal poles -flattening of corpus callosum	-abnormal white matter (decreased volume in parietal lobes) -possible focal dysgria -hypoplastic anterior temporal lobes -J-shaped sella	–
Head circumference (SD)	26 months, −2.21 3.75 years, −2.5	birth, −1.90 8.5 years −3.64	birth, −1.58 10 years, −2.47	6 months, +0.84 7.8 years, +0.3	5 weeks, −1.72 7 years, −1.50	birth, −1.27 4.6 years, −3.95	birth, −0.93 3 years, −2.13	birth, +0.31 4.25 years, −5.03	32 months, −4.05 15 years, −0.95	acquired microcephaly: 7/9
Height (SD)	birth, +0.70 3.75 years, −1.77	birth, +0.20 8.5 years, −1.50	birth, +0.62 10 years, −2.93	birth, +0.6 7.8 years, −1.56	5 weeks, −0.31 7 years, −0.12	birth, −1.26 4.6 years, −1.73	birth, −0.94 3 years, −0.68	birth, −0.44 4.25 years, −0.11	birth, −0.62 15 years, −1.23	–

(*Continued on next page*)

Table 1. *Continued*

	I-1	I-2	I-3	I-4	I-5	I-6	I-7	I-8	I-9	Total
Skeletal abnormalities	-coronal synostosis -mildly tapered fingers -5th finger clinodactyly	mildly tapered fingers	no	-prominent metopic ridge -mildly tapered fingers -coxa valga	no	-prominent metopic ridge -talipes equinovarus -prominent xyphoid process -short arms and hands	no	-scoliosis -small feet	-narrow fingers -distal camptodactyly -5th finger clinodactyly -pes planus -bent 3rd toes	6/9
Prominent maxilla/upper lip	yes	yes	yes	yes	yes	yes	yes	yes	yes	9/9
Micrognathia	no	yes	yes	yes	yes	yes	no	no	yes	6/9
Long ears	yes	yes	yes	yes	no	yes	no	yes	no	6/9

DEE, developmental and epileptic encephalopathy; SD, standard deviation; CVI, cerebral visual impairment; ND, not defined.
[a]mosaic variant

observation and in light of the known localization of PIP5KIγ to endosomes,[14] we co-stained cells with endosomal markers and found that PI(4,5)P2 is enriched in the EEA1-positive compartment (Figure 2B). We measured a 2.4-fold increase of PI(4,5)P2 levels specifically at the EEs marked by EEA1 (Figure 2B). We also measured the levels of the intracellular pool of PI4P, the substrate of the PIP5KIγ kinase, and did not observe any change in terms of amount and/or distribution between I-2 and control cells (Figure S2).

To evaluate the impact of all the identified PIP5KIγ protein variants on PI(4,5)P2 levels, we transfected constructs encoding the p.Glu146Lys, p.Tyr221Cys, and p.Tyr205Cys variants and the wild-type (WT) PIP5KIγ kinase into control fibroblasts and HeLa cells. As negative controls, we expressed the p.Asp253Asn loss-of-function mutant,[33] which causes LCCS3 in the homozygous state.

We first compared the protein levels of the mutants and WT PIP5KIγ kinase, and we measured the half-life of the different proteins. Immunoblot analysis on HeLa cell lysates expressing the FLAG-tagged mutant and WT proteins did not show any major effect on protein amounts, except for the p.Tyr205Cys mutant, which was expressed with lower efficiency (Figure S3A). In addition, the cycloheximide (CHX) chase analysis revealed that the p.Tyr205Cys, p.Tyr221Cys, and p.Glu146Lys variants show a comparable half-life (around 6 h) compared with WT PIP5KIγ (Figures S3B and S3B′). Conversely, a slower decay in p.Asp253Asn mutant amount was observed, compatible with increased stability of the loss-of-function mutant (Figures S3 and S3B′). These biochemical assays thus suggest that the *de novo* PIP5KIγ variants we identified did not impact either protein levels or stability.

We performed immunofluorescence experiments to measure the PI(4,5)P2 levels. The staining demonstrated that PI(4,5)P2 levels increased in PIP5KIγ p.Glu146Lys-, p.Tyr205Cys-, and p.Tyr221Cys-transfected cells compared with untransfected control fibroblasts (Figure S4A). The increased PI(4,5)P2 levels observed in p.Tyr205Cys-overexpressing cells confirmed the results obtained by quantification of the PI(4,5)P2 levels in I-2 fibroblasts. The overexpression of the WT PIP5KIγ resulted in increased PI(4,5)P2 levels (Figure S4A), as shown previously.[11] Conversely, fibroblasts overexpressing either the p.Asp253Asn variant or the empty vector showed PI(4,5)P2 amounts comparable with untransfected cells (Figure S4A). To further confirm these data, we used HeLa cells. When the *PIP5K1C* WT and mutants were expressed in similar amounts, we measured an increase in the PI(4,5)P2 levels in p.Glu146Lys-, p.Tyr205Cys-, and p.Tyr221Cys-transfected cells compared with the WT PIP5KIγ (Figure S4B). The overexpression of the WT PIP5KIγ resulted in increased PI(4,5)P2 levels compared with untransfected cells, as expected (Figure S4B). Conversely, cells overexpressing p.Asp253Asn showed PI(4,5)P2 levels completely overlapping to those of untransfected cells (Figure S4B). Altogether, these findings

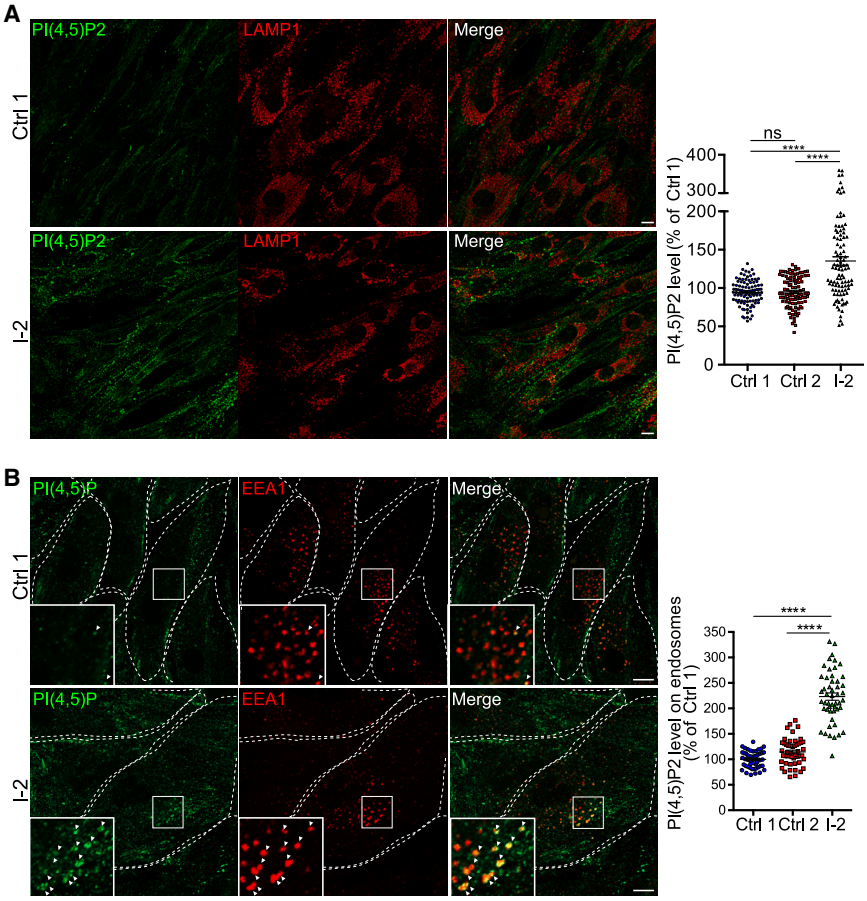

Figure 2. Mutant PIP5KIγ results in upregulation of PI(4,5)P2 levels and affects the PI composition of EEs

(A) Left: immunodetection of PI(4,5)P2 with an anti-PI(4,5)P2 antibody in control (Ctrl 1) and I-2 fibroblasts fixed and co-stained with an anti-LAMP1 antibody. Right: quantification of PI(4,5)P2 levels (the ratio of PI(4,5)P2 and LAMP1 fluorescence intensity) in I-2 fibroblasts and 2 unrelated controls (Ctrl 1 and 2), expressed as % of Ctrl 1. Means ± SEM, three independent experiments, n > 50 cells per experiment; Student's t test. ****p < 0.0001.

(B) Left: Airyscan confocal analysis of endogenous PI(4,5)P2 and EEA1 colocalization in I-2 fibroblasts and control (Ctrl 1). Green, PI(4,5)P2; red, EEA1. Insets show magnifications of selected areas. Scale bar, 10 μm. Right: quantification of PI(4,5)P2/EEA1 colocalization, expressed as % of Ctrl 1 (mean ± SD) in I-2 fibroblasts and controls. Three independent experiments, n > 50 cells per experiment; Student's t test. ****p < 0.0001; ns, not significant.

support the hypothesis that p.Glu146Lys, p.Tyr205Cys, and p.Tyr221Cys variants are more efficient in producing PI(4,5)P2.

Increased levels of PI(4,5)P2 cause F-actin polymerization defects

Actin dynamics are under the control of PI(4,5)P2,[45,46] and PIP5K overexpression alters both actin dynamics[47,48] and cell migration.[49] Thus, we asked whether increased PI(4,5)P2 levels associated with the *PIP5K1C* variants influence the actin cytoskeleton in the affected individuals. We observed an increased number of F-actin foci accumulated on internal membranes in I-2 fibroblasts compared with control cells (Figure 3). We further investigated the nature of the membranes and found that the actin foci co-localized with EEA1-positive compartments (Figure 3). At steady state, 80% of EEA1-positive endosomes in I-2 fibroblasts were associated with actin (Figure 3). Conversely, the percentage of EEs positive for F-actin in control cells (Ctrl1 and Ctrl2) was around 20%, 4-fold less than in I-2 cells (Figure 3).

We next asked whether fibroblasts overexpressing the other *PIP5K1C* variants also showed ectopic recruitment of F-actin on EEs, given the association with increased PI(4,5)P2 levels (Figure S5). Ectopic expression in WT fibroblasts of constructs expressing the variants and controls demonstrated that foci of F-actin accumulated on EE membranes in p.Glu146Lys-, p.Tyr205Cys-, p.Tyr221Cys-, and WT-transfected cells (Figure S5). As expected, fibroblasts overexpressing the p.Tyr205Cys PIP5KIγ kinase confirmed the abnormal recruitment of actin on EEs observed in I-2 fibroblasts. Conversely, fibroblasts overexpressing p.Asp253Asn or the empty vector did not show the endosomal-actin phenotype (Figure S5).

F-actin recruitment on EEs causes defects in endosomal trafficking

F-actin controls different steps of membrane trafficking ranging from internalization of receptors and their bound ligands to cargo sorting toward their final destinations and/or recycling back to the plasma membrane.[50,51] Because endosomes are central collecting stations in cells where different trafficking pathways converge, we asked whether the enhanced PI(4,5)P2 on EEs caused by the *PIP5K1C* variants may cause dysfunctional endosomal trafficking.

We analyzed the trafficking of Tf, a cargo widely used to study endosomal dynamics.[52] Tf is a protein that binds iron and promotes iron uptake by cells. Iron-loaded Tf binds the Tf receptor on the plasma membrane and is then internalized into the cell through endocytosis mediated by clathrin. After internalization, Tf is transported to EEs, delivers iron, and, with its receptor, is directed back to the cell surface by recycling endosomes.[53] This process occurs in the order of seconds to minutes. We administered Tf exogenously as a recombinant fluorescently conjugated ligand to fibroblasts from I-2 and control individuals and

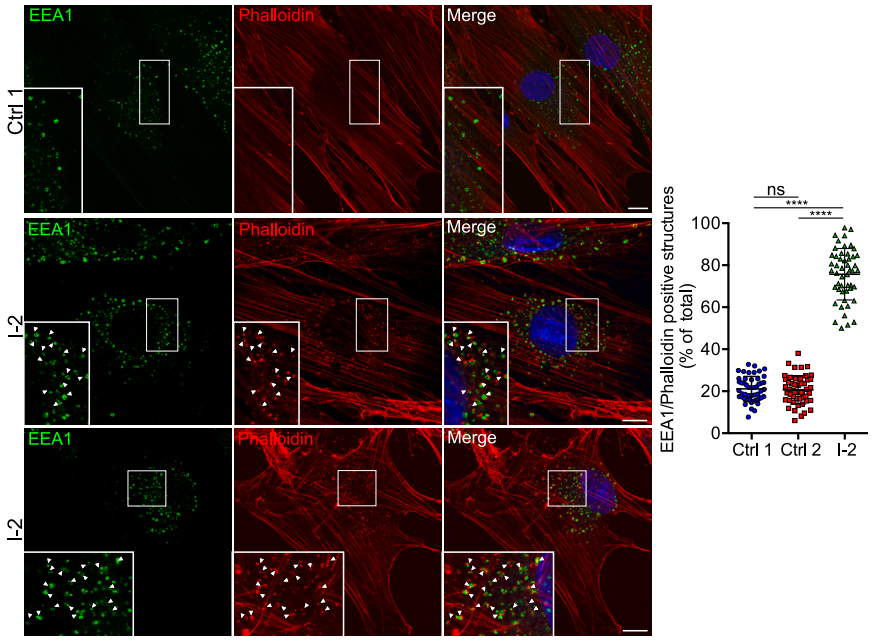

Figure 3. Mutant PIP5KIγ promotes ectopic recruitment of F-actin at EEs

Left: Airyscan confocal analysis of control and I-2 fibroblasts stained with Alexa-Fluor-phalloidin to visualize F-actin and with anti-EEA1 antibody to visualize EE compartments. Insets show enlargements of the boxed areas. White arrows indicate structures positive to phalloidin and EEA1 staining. Red, phalloidin; green, EEA1. Scale bar, 10 μm. Right: quantification of amounts of F-actin associated with endosomes is expressed as % of endosomes positive for F-actin ± SD Three independent experiments, n > 50 cells per experiment; Student's t test. ****p < 0.0001; ns, not significant.

incubated the cells at 4°C to allow binding to its receptor without allowing its internalization. Under these conditions, the Tf fluorescence was observed as a diffuse staining of the plasma membrane (Figure 4A), but Tf binding to the plasma membrane was reduced significantly in the I-2 fibroblasts compared with control individuals (Figure 4A). Because surface-bound Tf depends on the efficiency of the trafficking and recycling of its receptor by endosomes,[53] this result suggested that there might be a defect in Tf-receptor recycling/exposure. We then measured the ratio of internalized Tf on the bound fraction of Tf and observed that the rate of its internalization is comparable between I-2 and control cells (Figure 4A), suggesting that the internalization process is not affected in I-2 fibroblasts. Prompted by the observation that the Tf-receptor recycling step may be affected, we specifically analyzed the recycling processes. To this end, we loaded both control and I-2 fibroblasts with fluorescently labeled Tf continuously for 1 h at 37°C to allow ligand entry. We then removed Tf and observed its trafficking over time. I-2 cells showed slower recycling rates of the internalized Tf (Figure 4B) compared with control cells, suggesting that the reduced surface-bound Tf levels were due to impaired re-exposure of the Tf receptor on the cell surface.

Thus, a combination of both quantitative and qualitative analysis of Tf trafficking demonstrates that the mutant PIP5KIγ is associated with altered endosomal function.

Zebrafish mutant models resemble the human disease

To investigate *in vivo* the causal link between the neurological, ocular, and craniofacial defects observed in affected individuals and the variants found in *PIP5K1C*, we overexpressed the three human variants p.Glu146Lys, p.Tyr205Cys, and p.Tyr221Cys, as well as the WT and p.Asp253Asn forms and GFP as control, by injecting mRNA into zebrafish embryos at the one-cell stage. Initially, we injected different concentrations of these mRNA variants and the control GFP mRNA (50 ng/μL, 25 ng/μL, 20 ng/μL, and 10 ng/μL) and chose a concentration of 20 ng/μL, which showed a mortality rate between 27% and 57.5% (Figure S6), for further analysis. We then classified the injected embryos at 2 dpf in three different groups based on the severity of the observed morphological defects (Figure 5A). The first group, composed of morphologically "WT-like" embryos, did not display any aberrant phenotypes. The second group showed ocular abnormalities such as the development of one eye only or a small eye and/or microcephaly. Finally, the third group of embryos showed no eye development and extreme microcephaly (Figure 5A). Quantification of the morphological abnormalities revealed that overexpression of the WT PIP5K1C, PIP5K1C-p.Asp253Asn, and control (injected with GFP mRNA) resulted in less than 4%, 6%, and 5%, respectively, of the surviving embryos having an aberrant phenotype (Figure 5A′). Overexpression of the PIP5K1C-p.Glu146Lys variant resulted in 46% of the injected embryos having ocular abnormalities and/or microcephaly, and 3.4% showed no eyes and microcephaly (Figure 5A′). Overexpression of the PIP5K1C-p.Tyr205Cys variant caused ocular abnormalities and/or microcephaly in 32.7% of surviving embryos at 2 dpf and no eyes and microcephaly in 6.7% (Figure 5A′). Finally, with the overexpression of PIP5K1C-p.Tyr221Cys, 32% of the surviving embryos exhibited ocular abnormalities and/or microcephaly and 14% no eyes with microcephaly (Figure 5A′). Altogether, these results suggest that the human *PIP5K1C* variants are functionally relevant and that the neurodevelopmental defects observed in the affected individuals are caused by the variants identified in *PIP5K1C*.

To extend the analysis of the observed aberrant phenotypes and to assess whether these larvae show head structure defects similar to individuals from our cohort, we performed Alcian blue staining, which allowed visualization of head cartilage structures of the injected larvae at 3 dpf

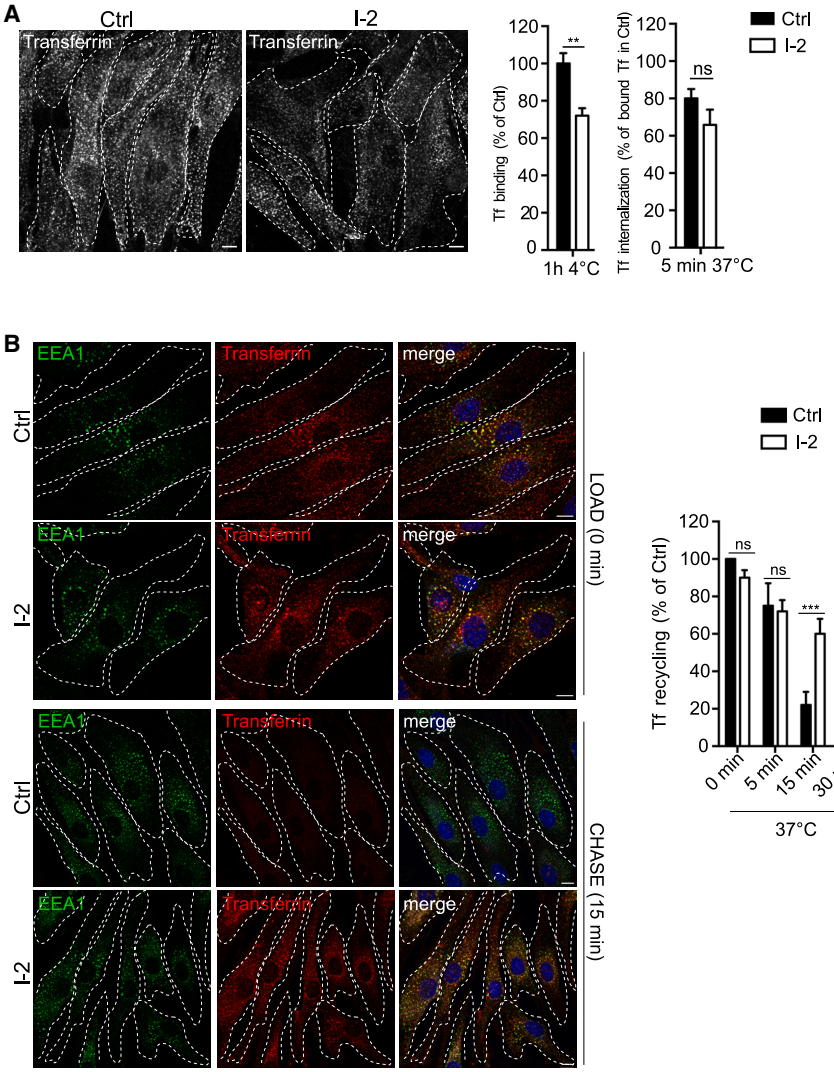

Figure 4. Mutant PIP5KIγ impairs Tf recycling

(A) Control (Ctrl) and I-2 fibroblasts were exposed to Alexa-Fluor-488-Tf for 1 h at 4°C and then warmed to 37°C in complete medium for 5 min. Left: representative confocal image of Tf bound to the plasma membrane in I-2 and control fibroblasts (1h at 4°C). Right: the first graph shows the quantification of cell-associated A488-Tf (1 h at 4°C) expressed as percentages of bound Tf at the plasma membrane in the control. The second graph shows the quantification of the fraction of internalized/bound Tf expressed as percentages of the control. Data are mean values ± SD (n > 50 cells per experiment; three independent experiments); **p ≤ 0.01.

(B) Control (Ctrl) and I-2 fibroblasts were loaded with Alexa-Fluor-488-Tf for 1 h at 37°C (LOAD) and chased in complete medium for 5, 15, and 30 min (CHASE). Left: representative confocal images of I-2 and control fibroblasts loaded for 1 h and chased for 15 min with Alexa-Fluor-488-Tf. Right: fluorescence intensities detected in the cells after 5, 15, and 30 min of chase were quantified and expressed as percentages of the loaded Tf in the control (0 min). Data are mean values ± Sd (n > 50 cells per experiment; three independent experiments). ***p ≤ 0.001; ns, not significant. Scale bar, 10 μm.

(Figure 5B). In all cases, the WT-like larvae and the larvae showing ocular abnormalities and/or microcephaly showed head cartilage structures, while the larvae from the third group with no eye development and severe microcephaly did not show any cartilage structures (Figure 5B). To quantify this phenotype, we measured the distance between Meckel's and ceratohyal cartilages along the antero-posterior axis of injected larvae. Overall, we observed that the distance between Meckel's and ceratohyal cartilages was smaller in the larvae injected with PIP5K1C-p.Glu146Lys-, PIP5K1C-p.Tyr205Cys-, and PIP5K1C-p.Tyr221Cys-encoding mRNAs showing an aberrant phenotype compared with the larvae injected with control *PIP5K1C*-WT mRNA (Figure 5B′, measure 1). We also measured the angle at the ceratohyal cartilage intersection, but no difference was observed between the variants and the WT control larvae (Figure 5B′, measure 2). These results highlight a reduction of the injected larvae heads and suggest a possible causative role of the human *PIP5K1C* variants in the aberrant head phenotype of the zebrafish mutant larvae.

To validate the causality link between human *PIP5K1C* variants and the aberrant mutant phenotypes, we developed a disease model by genetically introducing the corresponding human variants in the zebrafish genome to produce equivalent endogenous modifications in the zebrafish protein. The zebrafish genome has two *pip5k1c* genes, namely *pip5k1ca* and *pip5k1cb*. Pip5k1ca has 85% similarity and 71% identity with the human PIP5k1γ, while pip5k1cb has 75% similarity and 62% identity with the human counterpart. We performed *in situ* hybridization on the zebrafish larvae to assess whether the two zebrafish genes *pip5k1ca* and *pip5k1cb* show differential tissue expression. The *in situ* hybridization showed similar expression patterns, with both genes being broadly expressed in the head at 1 dpf and 2 dpf (Figure S7). To introduce the variants in the zebrafish genome, we used the CRIPSR-Cas9-based CBE system, which precisely generates C:G to T:A conversions thanks to the modified Cas9 nickase fused to the apolipoprotein B mRNA-editing enzyme catalytic subunit 1 (APOBEC1), a member of the cytidine deaminase enzyme family (Figure 5C), as described.[42,54] Of the three human variants, only the p.Glu146Lys variant could be introduced into zebrafish through the C:T conversion (Figure S8). We targeted *pip5k1ca* to introduce the p.Gly146Lys variant, which corresponds to the amino acid position Glu151 in

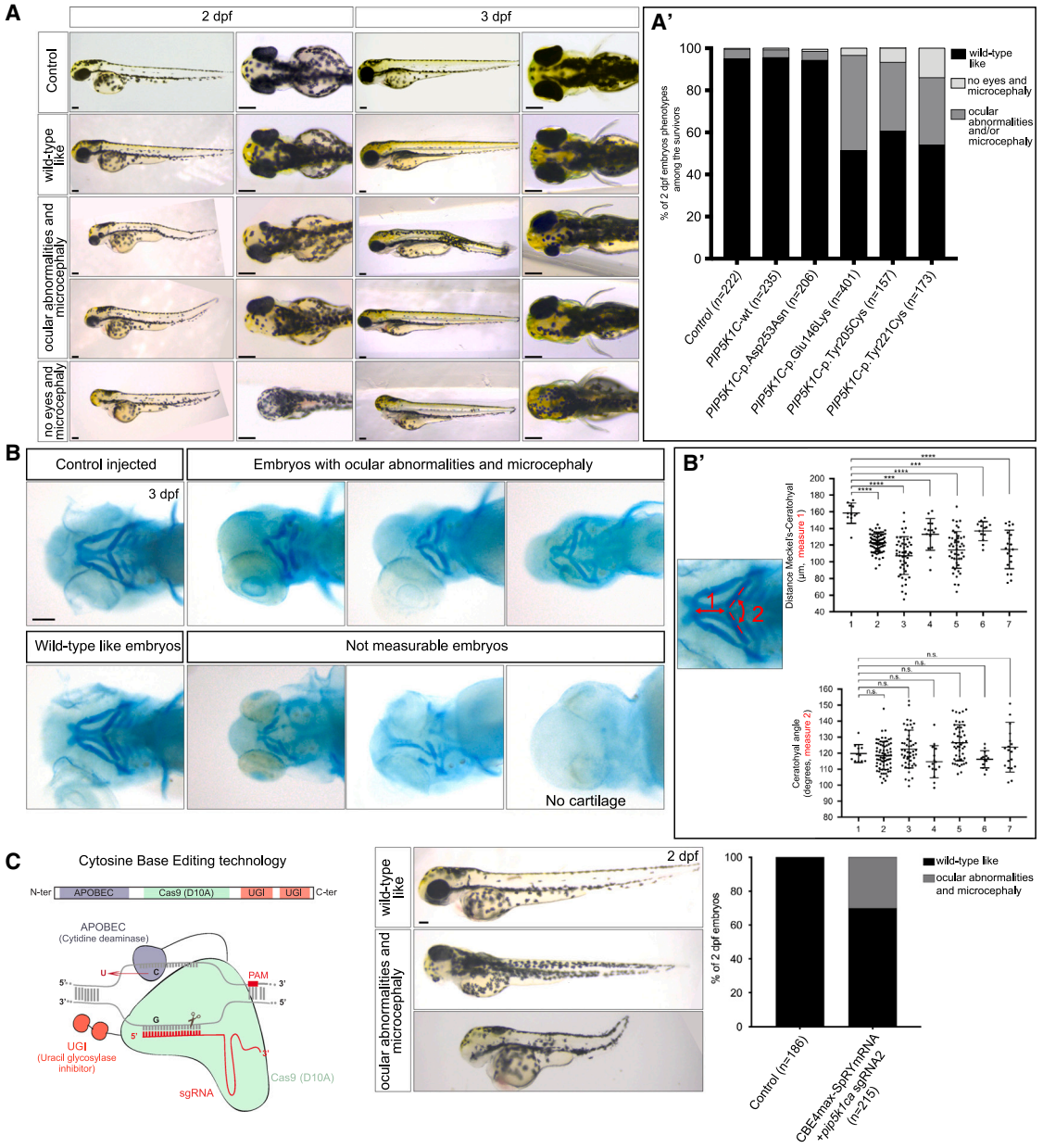

Figure 5. Disease-associated *PIP5K1C* variants in zebrafish induce developmental defects consistent with the human disease

(A) Phenotypes obtained in embryos at 2 and 3 dpf after injection of mRNAs encoding GFP (control), PIP5K1C-WT, PIP5K1C-p.Asp253Asn, PIP5K1C-p.Glu146Lys, PIP5K1C-p.Tyr205Cys, and PIP5K1C-p.Tyr221Cys mRNAs at 20 ng/μL in one-cell-stage embryos. Aberrant embryos present a spectrum of ocular abnormalities or no eyes and microcephaly. Scale bar, 50 μm.

(A′) Quantification of embryos showing the different phenotypes among the surviving embryos injected with mRNAs encoding GFP (control), PIP5K1C-WT, PIP5K1C-p.Asp253Asn, PIP5K1C-p.Glu146Lys, PIP5K1C-p.Tyr205Cys, and PIP5K1C-p.Tyr221Cys mRNAs. Total number of injected embryos per column is 222, 235, 206, 401, 157, and 173, respectively.

(B) Alcian blue staining of 3-dpf larvae injected with mRNAs encoding GFP (control), PIP5K1C-WT, PIP5K1C-p.Tyr205Cys, PIP5K1C-p.Tyr221Cys, and PIP5K1C-p.Glu146Lys mRNAs at 20 ng/μL showing aberrant head structures and WT phenotype. Scale bar, 150 μm.

(B′) Quantification of the distance between Meckel's and ceratohyal cartilages (measure 1) and the ceratohyal angle (measure 2). X axis: (1) PIP5K1C-WT, WT-like embryos (n = 11); (2) PIP5K1C-p.Glu146Lys, WT-like embryos (n = 72); (3) PIP5K1C-p.Glu146Lys, embryos with abnormalities (n = 50); (4) *PIP5K1C*-p.Tyr205Cys, WT-like embryos (n = 15); (5) PIP5K1C-p.Tyr205Cys, embryos with abnormalities (n = 47); (6) PIP5K1C-p.Tyr221Cys, WT-like embryos (n = 13); (7) PIP5K1C-p.Tyr221Cys, embryos with abnormalities (n = 20). Wilcoxon-Mann-Whitney test: ***$p < 0.001$, ****$p < 0.0001$; n.s., not significant.

(C) Left: schematic representation of the cytidine base editor technology. Middle: phenotypes obtained in the embryos mutated in *pip5k1ca* for the insertion of the p.Glu151Lys variant. Scale bar, 50 μm. Right: quantification of the embryos showing ocular abnormalities and microcephaly in control embryos (injected with CBE4max-SpRYmRNA, n = 186) and in the embryos injected for the insertion of the p.Glu151Lys variant (injected with CBE4max-SpRYmRNA +*pip5k1ca* sgRNA2, n = 215).

zebrafish. Upon injection of the modified Cas9 mRNA with the selected *pip5k1ca* sgRNA (see Figure S8), we obtained 30% of the injected embryos showing microphthalmia and/or microcephaly, the same phenotype obtained with the human mutated *PIP5K1C* mRNA overexpression (Figure 5C).

Discussion

PIs are important regulators of the membrane composition of different organelles and are produced through local activity of PI kinases and phosphates. They interact with a wide range of cytosolic proteins and play a key role in many cellular processes.[2]

A broad spectrum of inherited neurodevelopmental and neurodegenerative diseases are caused by mutations in PI-metabolizing enzymes. Examples include Lowe syndrome, Joubert syndrome, and MDCCAID, all resulting from mutations in PI(4,5)P2 phosphatase enzymes. In addition, mutations in genes encoding phosphatidylinositol 3-kinase (PIK3CA),[55] phosphoinositide-3-kinase regulatory subunit 2 (PIK3R2),[56] phosphatidylinositol 4-kinase (PIK4CA), and phosphoinositide 5-phosphatase (FIG4)[57] result in brain malformations such as polymicrogyria.[55] Mutations in phosphatidylinositol 3,4,5 trisphosphate 3-phosphatase (*PTEN*; MIM: 601728) are associated with macrocephaly, autism, poorly developed white matter, and reduced cognitive abilities.[58] These observations demonstrate the function of PIs in brain development.

Here, we describe a neurodevelopmental disorder associated with PI signaling dysfunction. We identified *de novo* heterozygous missense variants in *PIP5K1C* in nine unrelated children exhibiting intellectual disability, developmental delay, microcephaly, seizures, visual and ocular abnormalities, and dysmorphic features (see Table 1 and supplemental note for further details). The variants, located in the catalytic domain of the PIP5KIγ protein kinase, result in gain of function causing increased production of PI(4,5)2 in the affected individuals from our cohort. Prior to this report, in 2007, Narkis and colleagues described a form of LCCS3 characterized by congenital non-progressive contractures, akinesia and malformation of the limbs and joints, and degeneration of motoneurons, associated with a homozygous loss-of-function variant in *PIP5K1C* found in affected individuals from two unrelated consanguineous Israeli Bedouin families.[33] The homozygous variant caused substitution of aspartic acid by asparagine at amino acid 253 and in this case abrogated the kinase activity of PIP5KIγ, thus leading to decreased synthesis of PI(4,5)P2.[33] This reduction was postulated to cause defective synaptic vesicular trafficking and neuronal dysfunction.[33] Using biochemical assays, we showed that the *de novo* gain-of-function PIP5KIγ variants we identified did not impact either protein levels or stability. Conversely, an increased stability of the loss-of-function variant associated with LCCS3 was observed. Although gain-of-function variants are most commonly associated with protein-stabilizing effects, loss-of-function pathogenic missense variants enhancing the stability of the corresponding protein have been recently predicted by computational approaches,[59] even if with a much lower tendency, to be stabilizing with respect to gain-of-function or dominant-negative variants.[59]

Here, we provide evidence that specific *de novo* missense variants of *PIP5K1C* are associated with a disorder resulting in an increase in the endosomal PI(4,5)P2 pool, which causes ectopic recruitment of F-actin at EEs that in turn is detrimental for EE trafficking. The PIP5KIγ enzyme can be targeted to distinct cellular compartments.[13,14] It was found to localize to the plasma membrane, focal adhesions, and adherent junctions;[11,12] to early, late, and recycling endosomes; and to lysosomes and in the nucleus.[13,14] We cannot exclude that *PIP5K1C* variants influence the subcellular distribution of the PIP5KIγ enzyme and the physical binding between PIP5KIγ and its interactors. These changes could also induce enrichment of the PI(4,5)P2 pool on other subcellular compartments in addition to the EEs and thus be associated with the altered lysosomal dynamics and function or with aberrant focal adhesion plaque formation. Consequently, it cannot be excluded that increased PI(4,5)P2 production at other subcellular compartments[20] could contribute to the phenotype we observed. However, our findings are in line with previous observation of cellular models of Lowe syndrome, characterized by increased PI(4,5)P2 levels caused by mutations occurring in the 5-phosphatase OCRL.[31,60–62] Vicinanza and colleagues demonstrated that loss of the 5-phosphatase activity of OCRL results in an accumulation of PI(4,5)P2 at EE membranes, which leads to increased association of F-actin at EEs, affecting EE function in cellular models of Lowe syndrome.[31] These findings are consistent with the observation that actin dynamics are under the strict control of PI(4,5)P2, as reported by several groups over the years.[45,46,63] The first link was established thanks to the observation that overexpression of PIP5K altered actin dynamics, leading to the dissolution of stress fibers,[64] the formation of motile actin comets,[47] cell rounding,[48] and increased cell migration[49] as a result of the local increase in the levels of PI(4,5)P2 at the plasma membrane. The role for PI(4,5)P2 in regulating the actin cytoskeleton was then confirmed when a large number of PI(4,5)P2-interacting proteins controlling actin cytoskeleton were identified.[46,65,66] Subsequently, the functional link between PIP5K and the actin cytoskeleton has been studied extensively.

Because *OCRL* depletion has been shown to result in endosomal dysfunction induced by PI(4,5)P2-mediated recruitment of F-actin at EEs,[31] we asked whether the increased PI(4,5)P2 on EEs associated with *PIP5K1C* variants may cause similar dysfunction in endosomal trafficking.

Indeed, we demonstrated, through analysis of Tf-trafficking routes in I-2 fibroblasts, that the p.Tyr205Cys

PIP5KIγ variant impairs endosomal recycling. While some receptors and ligands are endocytosed and trafficked to the lysosomes, Tf is transported back to the plasma membrane through the recycling pathway. Proper homeostasis of membrane proteins, including receptors, adhesion anchors, and enzymes of the plasma membrane, is essential for proper brain development. Moreover, regular trafficking of membrane proteins is required for synaptic plasticity in neurons.[67] Thus, impairment in endosomal recycling is likely to influence synaptic communications and brain developmental processes and to cause neurological and neurodevelopmental disorders in humans. Our findings are in line with several studies demonstrating a key role of PIs in brain function and development. PI(4,5)P2 levels control both exocytosis and endocytosis at synaptic vesicle membranes.[68] Furthermore, PIP5KIγ kinase is a major regulator in maintaining appropriate levels of the neuronal synaptic pool of PI(4,5)P2 and is essential for synaptic transmission and synaptic-vesicle trafficking.[20,21] Di Paolo and colleagues showed that *Pip5k1c*$^{-/-}$ mice exhibit major neurological and/or behavioral defects associated with early postnatal lethality resulting from impaired synaptic vesicle trafficking.[21] Wang et al. showed that mice lacking PIP5K1γ had pleiotropic developmental defects and embryonic lethality due to failure in proper cardiac chamber septation and neural tube closure defects.[69]

We established a gain-of-function model in zebrafish (*Danio rerio*) for the developmental disorder we describe. By injecting human mutant *PIP5K1C* mRNA displaying the three different variants, we observed a high mortality rate, suggesting that the aberrant proteins have toxic effects, which may explain the rarity of individuals with variants in *PIP5K1C*. We also genetically introduced one of the three human variants into the zebrafish genome by the CRIPSR-Cas9-based CBE system. The zebrafish genome has two *pip5k1c* genes, *pip5k1ca* and *pip5k1cb*, with similar expression (Figure S7). We chose to target only *pip5k1ca* due to the higher similarity with the human PIP5KIγ. As the three *PIP5K1C* variants act as gain-of-function mutations, we reasoned that altering only one of the two genes would be sufficient to analyze the effect of the variants, as it would result in a dominant and constitutively active form of the protein. The zebrafish models we generated showed microcephaly, ocular abnormalities, and altered head cartilage structure. The zebrafish larvae phenotypes recapitulating the phenotypes of the affected individuals demonstrate the pathogenic effect of the three *de novo* missense variants. Our *in vivo* models confirm the pivotal role of *PIP5K1C* in the development of neuronal structures, as also shown with the *Pip5k1c*$^{-/-}$ mice.[21,69] However, the mechanistic link bridging these *PIP5K1C* gain-of-function variants reported here and the clinical manifestation of this neurodevelopmental disorder remain to be determined and need to be explored in neuronal tissue.

The craniofacial abnormalities seen in the affected individuals and zebrafish models we describe point to a role of *PIP5K1C* in craniofacial patterning. The underlying mechanism is unknown, although PI(4,5)P2 has been shown to interact with the histone lysine demethylase PHF8,[70] a transcription activator known to be involved in the regulation of craniofacial and brain development in zebrafish.[71] In addition, loss of function in *PHF8* causes a syndromic form of X-linked intellectual disability with dysmorphic facial features.[72] Furthermore, PI(4,5)P2 is a key substrate for phospholipase C-γ (PLCG1) and phosphatidylinositol 3 kinases, which mediate downstream signaling activation of multiple receptors including the fibroblast growth factor receptor 1 (FGF1R),[73] which plays a major role in craniofacial development.[74]

The phenotypes we see in the affected individuals with gain-of-function variants in *PIP5K1C* are similar to those seen with loss-of-function variants in *INPP5K*, which codes for the inositol polyphosphate-5-phosphatase K. Like the *PIP5K1C* gain-of-function variants, *INPP5K* loss-of-function variants also cause increased PI(4,5)P2 levels. Upon growth factor or insulin stimulation, INPP5K protein translocates from the endoplasmic reticulum to the plasma membrane where it interacts with sub-membranous actin and membrane ruffles.[75] Mutations that impair phosphatase activity or alter *INPP5K* subcellular localization can lead to congenital muscular dystrophy, early onset cataracts, mild-to-moderate intellectual disability, microcephaly, epilepsy, and short stature.[25,76] *INPP5K* loss of function in the zebrafish results in shortened body axis, microphthalmia, microcephaly, reduced touch-evoked motility, and highly disorganized myofibers.[26] Increased PI(4,5)P2 levels could underlie the motor delays and hypotonia seen in our cohort. An intriguing hypothesis that remains to be proven is that PI(4,5)P2 phosphatases may serve to counterbalance *PIP5K1C* function.

From a clinical point of view, PIP5Ks represent attractive therapeutic targets. Reduction in PI(4,5)P2 production, by reducing PIP5Ka levels, also attenuates the disruption of endocytic trafficking due to *OCRL* loss, suggesting that PIP5Ka may be a promising target for pharmacological treatment of Lowe syndrome.[31] In addition, PIPK-specific inhibitors,[9] including a small-molecule inhibitor of PIP5KIγ,[77] may be therapeutic tools for persons with disorders associated with increased PI(4,5)P2 levels.

Consortia

Members of the Undiagnosed Diseases Network include Maria T. Acosta, Margaret Adam, David R. Adams, Raquel L. Alvarez, Justin Alvey, Laura Amendola, Ashley Andrews, Euan A. Ashley, Carlos A. Bacino, Guney Bademci, Ashok Balasubramanyam, Dustin Baldridge, Jim Bale, Michael Bamshad, Deborah Barbouth, Pinar Bayrak-Toydemir, Anita Beck, Alan H. Beggs, Edward Behrens, Gill Bejerano, Hugo J. Bellen, Jimmy Bennett, Beverly Berg-Rood, Jonathan A. Bernstein, Gerard T. Berry, Anna Bican, Stephanie Bivona, Elizabeth Blue, John Bohnsack, Devon Bonner, Lorenzo Botto, Brenna Boyd, Lauren C. Briere, Gabrielle

Brown, Elizabeth A. Burke, Lindsay C. Burrage, Manish J. Butte, Peter Byers, William E. Byrd, John Carey, Olveen Carrasquillo, Thomas Cassini, Ta Chen Peter Chang, Sirisak Chanprasert, Hsiao-Tuan Chao, Gary D. Clark, Terra R. Coakley, Laurel A. Cobban, Joy D. Cogan, Matthew Coggins, F. Sessions Cole, Heather A. Colley, Cynthia M. Cooper, Heidi Cope, Rosario Corona, William J. Craigen, Andrew B. Crouse, Michael Cunningham, Precilla D'Souza, Hongzheng Dai, Surendra Dasari, Joie Davis, Jyoti G. Dayal, Esteban C. Dell'Angelica, Katrina Dipple, Daniel Doherty, Naghmeh Dorrani, Argenia L. Doss, Emilie D. Douine, Dawn Earl, David J. Eckstein, Lisa T. Emrick, Christine M. Eng, Marni Falk, Elizabeth L. Fieg, Paul G. Fisher, Brent L. Fogel, Irman Forghani, William A. Gahl, Ian Glass, Bernadette Gochuico, Page C. Goddard, Rena A. Godfrey, Katie Golden-Grant, Alana Grajewski, Don Hadley, Sihoun Hahn, Meghan C. Halley, Rizwan Hamid, Kelly Hassey, Nichole Hayes, Frances High, Anne Hing, Fuki M. Hisama, Ingrid A. Holm, Jason Hom, Martha Horike-Pyne, Alden Huang, Sarah Hutchison, Wendy Introne, Rosario Isasi, Kosuke Izumi, Fariha Jamal, Gail P. Jarvik, Jeffrey Jarvik, Suman Jayadev, Orpa Jean-Marie, Vaidehi Jobanputra, Lefkothea Karaviti, Shamika Ketkar, Dana Kiley, Gonench Kilich, Shilpa N. Kobren, Isaac S. Kohane, Jennefer N. Kohler, Susan Korrick, Mary Kozuira, Deborah Krakow, Donna M. Krasnewich, Elijah Kravets, Seema R. Lalani, Byron Lam, Christina Lam, Brendan C. Lanpher, Ian R. Lanza, Kimberly LeBlanc, Brendan H. Lee, Roy Levitt, Richard A. Lewis, Pengfei Liu, Xue Zhong Liu, Nicola Longo, Sandra K. Loo, Joseph Loscalzo, Richard L. Maas, Ellen F. Macnamara, Calum A. MacRae, Valerie V. Maduro, AudreyStephannie Maghiro, Rachel Mahoney, May Christine V. Malicdan, Laura A. Mamounas, Teri A. Manolio, Rong Mao, Kenneth Maravilla, Ronit Marom, Gabor Marth, Beth A. Martin, Martin G. Martin, Julian A. Martínez-Agosto, Shruti Marwaha, Jacob McCauley, Allyn McConkie-Rosell, Alexa T. McCray, Elisabeth McGee, Heather Mefford, J. Lawrence Merritt, Matthew Might, Ghayda Mirzaa, Eva Morava, Paolo Moretti, John Mulvihill, Mariko Nakano-Okuno, Stanley F. Nelson, John H. Newman, Sarah K. Nicholas, Deborah Nickerson, Shirley Nieves-Rodriguez, Donna Novacic, Devin Oglesbee, James P. Orengo, Laura Pace, Stephen Pak, J. Carl Pallais, Christina G.S. Palmer, Jeanette C. Papp, Neil H. Parker, John A. Phillips III, Jennifer E. Posey, Lorraine Potocki, Barbara N. Pusey Swerdzewski, Aaron Quinlan, Deepak A. Rao, Anna Raper, Wendy Raskind, Genecee Renteria, Chloe M. Reuter, Lynette Rives, Amy K. Robertson, Lance H. Rodan, Jill A. Rosenfeld, Natalie Rosenwasser, Francis Rossignol, Maura Ruzhnikov, Ralph Sacco, Jacinda B. Sampson, Mario Saporta, Judy Schaechter, Timothy Schedl, Kelly Schoch, Daryl A. Scott, C. Ron Scott, Vandana Shashi, Jimann Shin, Edwin K. Silverman, Janet S. Sinsheimer, Kathy Sisco, Edward C. Smith, Kevin S. Smith, Lilianna Solnica-Krezel, Ben Solomon, Rebecca C. Spillmann, Joan M. Stoler, Kathleen Sullivan, Jennifer A. Sullivan, Angela Sun, Shirley Sutton, David A. Sweetser, Virginia Sybert, Holly K. Tabor, Queenie K.-G. Tan, Amelia L.M. Tan, Mustafa Tekin, Fred Telischi, Willa Thorson, Cynthia J. Tifft, Camilo Toro, Alyssa A. Tran, Rachel A. Ungar, Tiina K. Urv, Adeline Vanderver, Matt Velinder, Dave Viskochil, Tiphanie P. Vogel, Colleen E. Wahl, Melissa Walker, Stephanie Wallace, Nicole M. Walley, Jennifer Wambach, Jijun Wan, Lee-kai Wang, Michael F. Wangler, Patricia A. Ward, Daniel Wegner, Monika Weisz Hubshman, Mark Wener, Tara Wenger, Monte Westerfield, Matthew T. Wheeler, Jordan Whitlock, Lynne A. Wolfe, Kim Worley, Changrui Xiao, Shinya Yamamoto, John Yang, Zhe Zhang, Stephan Zuchner.

Members of the Telethon Undiagnosed Diseases Program include Vincenzo Nigro, Annalaura Torella, Manuela Morleo, Carmine Spampanato, Michele Pinelli, Sandro Banfi, Alessandra Varavallo, Angelo Selicorni, Milena Mariani, Marta Massimello, Cecilia Daolio, Valeria Capra, Andrea Accogli, Marcello Scala, Vincenzo Leuzzi, Francesca Nardecchia, Serena Galosi, Mario Mastrangelo, Donatella Milani, Giuseppina Vitiello, Giulio Piluso, Corrado Romano, Pinella Failla, Donatella Greco, Chiara Pantaleoni, Claudia Ciaccio, Stefano D'Arrigo, Nicola Brunetti Pierri, Giancarlo Parenti, Antonietta Coppola, Teresa Mattina, Marcella Zollino, Simona Amenta, Albina Tummolo, Claudia Santoro, Anna Grandone, Daniele De Brasi, Antonio Varone, Livia Garavelli, Carla Marini, Stefania Bigoni, Carmelo Piscopo, Antonio Trabacca, Marta De Rinaldis, Angela Peron.

Data and code availability

The variants c.436G>A (p.Glu146Lys), c.662A>G (p.Tyr221Cys), and c.614A>G (p.Tyr205Cys) have been submitted to ClinVar and can be found under the accession numbers VCV001172539, VCV001172538, and VCV001809611.

Supplemental information

Supplemental information can be found online at https://doi.org/10.1016/j.ajhg.2023.06.012.

Acknowledgments

The authors are grateful to affected individuals and their families. This work was supported by Combined Annotation Diseases Program (GSP15001), Solve-RD project (European Union's Horizon 2020 Research and Innovation Program no.779257), Tuscany Region Call for Health 2018 (DECODE-EE to R.G.), Fondazione Cassa di Risparmio di Firenze (Human Brain Project to R.G.), Programme Investissements d'Avenir IHU FOReSIGHT (ANR-18-IAHU-01 to F.D.B.), Agence Nationale de la Recherche (ANR-18-CE16-0017-01 IPOGUT, ANR-20-CE17-0020-02 INCEPTION, ANR-22-CE17-028 PEMGeT to F.D.B.), Fondation pour la Recherche Médicale (MND202003011485 to F.D.B., ECO20170637481 to M.R.), La Ligue Nationale contre le Cancer. V.P., T.A., and J.A. were supported by France Genomic Medicine Plan 2025 (SeqOIA) and R.V. by Italian Association for Cancer Research (MFAG 2020_25174). This work was supported by NIH Common Fund through the Office of Strategic Coordination/Office of the NIH Director no. U01HG007690 (E.T., L.C.B., F.A.H., M.A.W., D.A.S.,

L.H.R.). The content is the responsibility of the authors and does not necessarily represent the official views of the NIH. The Hill Family Fund for the Diagnosis and Management of Rare and Undiagnosed Diseases at Mass General, the American Institute for Neuro Integrative Development Inc (AIND), and a donation by Seta and Douglas Atamian supported this work (E.T., L.C.B., F.A.H., M.A.W., D.A.S.). The Translational Clinical Research Center at Massachusetts General Hospital was supported by NIH grant 1UL1TR001102. This study makes use of data shared/provided through RD-Connect, funded from the European Union Seventh Framework Programme (FP7/2007-2013, no.305444). We thank Emily Place, MS (Massachusetts Mass Eye and Ear) for the ophthalmological counseling and the TIGEM Bioinformatic Core.

Declaration of interests

The authors declare no competing interests.

Received: January 24, 2023
Accepted: June 22, 2023
Published: July 13, 2023

Web resources

BrainSpan, https://www.brainspan.org/rnaseq/search/index.html
CADD, https://cadd.gs.washington.edu/snv
ClinVar, https://www.ncbi.nlm.nih.gov/clinvar/
Ensembl, https://useast.ensembl.org/index.html
Franklin, https://franklin.genoox.com/clinical-db/home
GeneMatcher, https://genematcher.org/
gnomAD, https://gnomad.broadinstitute.org/
GTEx, https://gtexportal.org/home/
Illustrator for Biological Sequences, http://ibs.biocuckoo.org/
Marrvel, http://marrvel.org/
NCBI HomoloGene, https://www.ncbi.nlm.nih.gov/homologene
OMIM, https://www.omim.org/
PolyPhen-2, http://genetics.bwh.harvard.edu/pph2/
PyMOL, https://pymol.org/2/
UniProt, https://www.uniprot.org/

References

1. di Paolo, G., and de Camilli, P. (2006). Phosphoinositides in cell regulation and membrane dynamics. Nature *443*, 651–657.
2. Downes, C.P., Gray, A., and Lucocq, J.M. (2005). Probing phosphoinositide functions in signaling and membrane trafficking. Trends Cell Biol. *15*, 259–268.
3. Wu, C.Y., Lin, M.W., Wu, D.C., Huang, Y.B., Huang, H.T., and Chen, C.L. (2014). The role of phosphoinositide-regulated actin reorganization in chemotaxis and cell migration. Br. J. Pharmacol. *171*, 5541–5554.
4. Posor, Y., Eichhorn-Grünig, M., and Haucke, V. (2015). Phosphoinositides in endocytosis. Biochim. Biophys. Acta *1851*, 794–804.
5. Sechi, A.S., and Wehland, J. (2000). The actin cytoskeleton and plasma membrane connection: PtdIns(4,5)P2 influences cytoskeletal protein activity at the plasma membrane. J. Cell Sci. *113*, 3685–3695.
6. Cremona, O., and de Camilli, P. (2001). Phosphoinositides in membrane traffic at the synapse. J. Cell Sci. *114*, 1041–1052.
7. Toker, A. (1998). The synthesis and cellular roles of phosphatidylinositol 4,5-bisphosphate. Curr. Opin. Cell Biol. *10*, 254–261.
8. Kolay, S., Basu, U., and Raghu, P. (2016). Control of diverse subcellular processes by a single multi-functional lipid phosphatidylinositol 4,5-bisphosphate [PI(4,5)P2]. Biochem. J. *473*, 1681–1692.
9. van den Bout, I., and Divecha, N. (2009). PIP5K-driven PtdIns(4,5) P 2 synthesis: regulation and cellular functions. J. Cell Sci. *122*, 3837–3850.
10. Funakoshi, Y., Hasegawa, H., and Kanaho, Y. (2011). Regulation of PIP5K activity by Arf6 and its physiological significance. J. Cell. Physiol. *226*, 888–895.
11. di Paolo, G., Pellegrini, L., Letinic, K., Cestra, G., Zoncu, R., Voronov, S., Chang, S., Guo, J., Wenk, M.R., and de Camilli, P. (2002). Recruitment and regulation of phosphatidylinositol phosphate kinase type 1γ by the FERM domain of talin. Nature *420*, 85–89.
12. Ling, K., Doughman, R.L., Firestone, A.J., Bunce, M.W., and Anderson, R.A. (2002). Type Iγ phosphatidylinositol phosphate kinase targets and regulates focal adhesions. Nature *420*, 89–93.
13. Schill, N.J., and Anderson, R.A. (2009). Two novel phosphatidylinositol-4-phosphate 5-kinase type Igamma splice variants expressed in human cells display distinctive cellular targeting. Biochem. J. *422*, 473–482.
14. Sun, Y., Hedman, A.C., Tan, X., Schill, N.J., and Anderson, R.A. (2013). Endosomal Type Iγ PIP 5-Kinase Controls EGF Receptor Lysosomal Sorting. Dev. Cell *25*, 144–155.
15. el Sayegh, T.Y., Arora, P.D., Ling, K., Laschinger, C., Janmey, P.A., Anderson, R.A., and McCulloch, C.A. (2007). Phosphatidylinositol-4,5 bisphosphate produced by PIP5KIγ regulates gelsolin, actin assembly, and adhesion strength of N-cadherin junctions. Mol. Biol. Cell *18*, 3026–3038.
16. Kahlfeldt, N., Vahedi-Faridi, A., Koo, S.J., Schäfer, J.G., Krainer, G., Keller, S., Saenger, W., Krauss, M., and Haucke, V. (2010). Molecular basis for association of PIPKIγ-p90 with clathrin adaptor AP-2. J. Biol. Chem. *285*, 2734–2749.
17. Ling, K., Bairstow, S.F., Carbonara, C., Turbin, D.A., Huntsman, D.G., and Anderson, R.A. (2007). Type I gamma phosphatidylinositol phosphate kinase modulates adherens junction and E-cadherin trafficking via a direct interaction with mu 1B adaptin. J. Cell Biol. *176*, 343–353.
18. Schill, N.J., Hedman, A.C., Choi, S., and Anderson, R.A. (2014). Isoform 5 of PIPKIγ regulates the endosomal trafficking and degradation of E-cadherin. J. Cell Sci. *127*, 2189–2203.
19. Hara, Y., Fukaya, M., Tamaki, H., and Sakagami, H. (2013). Type I phosphatidylinositol 4-phosphate 5-kinase γ is required for neuronal migration in the mouse developing cerebral cortex. Eur. J. Neurosci. *38*, 2659–2671.
20. Wenk, M.R., Pellegrini, L., Klenchin, V.A., di Paolo, G., Chang, S., Daniell, L., Arioka, M., Martin, T.F., and de Camilli, P. (2001). PIP kinase Iγ is the major PI(4,5)P2 synthesizing enzyme at the synapse. Neuron *32*, 79–88.
21. di Paolo, G., Moskowitz, H.S., Gipson, K., Wenk, M.R., Voronov, S., Obayashi, M., Flavell, R., Fitzsimonds, R.M., Ryan, T.A., and De Camilli, P. (2004). Impaired PtdIns(4,5)P2 synthesis in nerve terminals produces defects in synaptic vesicle trafficking. Nature *431*, 415–422.
22. Wang, H.Y., Li, Y., Xue, T., Cheng, N., and Du, H.N. (2016). Construction of a series of pCS2+ backbone-based Gateway

vectors for overexpressing various tagged proteins in vertebrates. Acta Biochim. Biophys. Sin. *48*, 1128–1134.

23. de Matteis, M.A., Staiano, L., Emma, F., and Devuyst, O. (2017). The 5-phosphatase OCRL in Lowe syndrome and Dent disease 2. Nat. Rev. Nephrol. *13*, 455–470.
24. Travaglini, L., Brancati, F., Silhavy, J., Iannicelli, M., Nickerson, E., Elkhartoufi, N., Scott, E., Spencer, E., Gabriel, S., Thomas, S., et al. (2013). Phenotypic spectrum and prevalence of INPP5E mutations in Joubert Syndrome and related disorders. Eur. J. Hum. Genet. *21*, 1074–1078.
25. Wiessner, M., Roos, A., Munn, C.J., Viswanathan, R., Whyte, T., Cox, D., Schoser, B., Sewry, C., Roper, H., Phadke, R., et al. (2017). Mutations in INPP5K , Encoding a Phosphoinositide 5-Phosphatase, Cause Congenital Muscular Dystrophy with Cataracts and Mild Cognitive Impairment. Am. J. Hum. Genet. *100*, 523–536.
26. Osborn, D.P.S., Pond, H.L., Mazaheri, N., Dejardin, J., Munn, C.J., Mushref, K., Cauley, E.S., Moroni, I., Pasanisi, M.B., Sellars, E.A., et al. (2017). Mutations in INPP5K Cause a Form of Congenital Muscular Dystrophy Overlapping Marinesco-Sjögren Syndrome and Dystroglycanopathy. Am. J. Hum. Genet. *100*, 537–545.
27. Mehta, Z.B., Pietka, G., and Lowe, M. (2014). The cellular and physiological functions of the lowe syndrome protein OCRL1. Traffic *15*, 471–487.
28. Schmid, A.C., Wise, H.M., Mitchell, C.A., Nussbaum, R., and Woscholski, R. (2004). Type II phosphoinositide 5-phosphatases have unique sensitivities towards fatty acid composition and head group phosphorylation. FEBS Lett. *576*, 9–13.
29. Kisseleva, M.V., Wilson, M.P., and Majerus, P.W. (2000). The Isolation and Characterization of a cDNA Encoding Phospholipid-specific Inositol Polyphosphate 5-Phosphatase. J. Biol. Chem. *275*, 20110–20116.
30. Prosseda, P.P., Luo, N., Wang, B., Alvarado, J.A., Hu, Y., and Sun, Y. (2017). Loss of OCRL increases ciliary PI(4,5)P2 in oculocerebrorenal syndrome of Lowe. J. Cell Sci. *130*, 3447–3454. https://doi.org/10.1242/jcs.200857.
31. Vicinanza, M., Di Campli, A., Polishchuk, E., Santoro, M., Di Tullio, G., Godi, A., Levtchenko, E., De Leo, M.G., Polishchuk, R., Sandoval, L., et al. (2011). OCRL controls trafficking through early endosomes via PtdIns4,5P $_2$ -dependent regulation of endosomal actin. EMBO J. *30*, 4970–4985.
32. Chávez, M., Ena, S., Van Sande, J., de Kerchove d'Exaerde, A., Schurmans, S., and Schiffmann, S.N. (2015). Modulation of Ciliary Phosphoinositide Content Regulates Trafficking and Sonic Hedgehog Signaling Output. Dev. Cell *34*, 338–350. https://doi.org/10.1016/j.devcel.2015.06.016.
33. Narkis, G., Ofir, R., Landau, D., Manor, E., Volokita, M., Hershkowitz, R., Elbedour, K., and Birk, O.S. (2007). Lethal Contractural Syndrome Type 3 (LCCS3) Is Caused by a Mutation in PIP5K1C, Which Encodes PIPKIγ of the Phophatidylinsitol Pathway. Am. J. Hum. Genet. *81*, 530–539.
34. Philippakis, A.A., Azzariti, D.R., Beltran, S., Brookes, A.J., Brownstein, C.A., Brudno, M., Brunner, H.G., Buske, O.J., Carey, K., Doll, C., et al. (2015). The Matchmaker Exchange: A Platform for Rare Disease Gene Discovery. Hum. Mutat. *36*, 915–921.
35. Sobreira, N., Schiettecatte, F., Valle, D., and Hamosh, A. (2015). GeneMatcher: A Matching Tool for Connecting Investigators with an Interest in the Same Gene. Hum. Mutat. *36*, 928–930.
36. Kircher, M., Witten, D.M., Jain, P., O'roak, B.J., Cooper, G.M., and Shendure, J. (2014). A general framework for estimating the relative pathogenicity of human genetic variants. Nat. Genet. *46*, 310–315.
37. Kopanos, C., Tsiolkas, V., Kouris, A., Chapple, C.E., Albarca Aguilera, M., Meyer, R., and Massouras, A. (2019). VarSome: the human genomic variant search engine. Bioinformatics *35*, 1978–1980.
38. Adzhubei, I.A., Schmidt, S., Peshkin, L., Ramensky, V.E., Gerasimova, A., Bork, P., Kondrashov, A.S., and Sunyaev, S.R. (2010). A method and server for predicting damaging missense mutations. Nat. Methods *7*, 248–249.
39. Sim, N.L., Kumar, P., Hu, J., Henikoff, S., Schneider, G., and Ng, P.C. (2012). SIFT web server: Predicting effects of amino acid substitutions on proteins. Nucleic Acids Res. *40*. W452–W457.
40. Karczewski, K.J., Francioli, L.C., Tiao, G., Cummings, B.B., Alföldi, J., Wang, Q., Collins, R.L., Laricchia, K.M., Ganna, A., Birnbaum, D.P., et al. (2020). The mutational constraint spectrum quantified from variation in 141,456 humans. Nature *581*, 434–443.
41. Hammond, G.R.V., Schiavo, G., and Irvine, R.F. (2009). Immunocytochemical techniques reveal multiple, distinct cellular pools of PtdIns4P and PtdIns(4,5)P2. Biochem. J. *422*, 23–35.
42. Rosello, M., Serafini, M., Mignani, L., Finazzi, D., Giovannangeli, C., Mione, M.C., Concordet, J.-P., and del Bene, F. (2022). Disease modeling by efficient genome editing using a near PAM-less base editor in vivo. Nat. Commun. *13*, 3435.
43. Kluesner, M.G., Nedveck, D.A., Lahr, W.S., Garbe, J.R., Abrahante, J.E., Webber, B.R., and Moriarity, B.S. (2018). EditR: A Method to Quantify Base Editing from Sanger Sequencing. CRISPR J *1*, 239–250.
44. Walker, M.B., and Kimmel, C.B. (2007). A two-color acid-free cartilage and bone stain for zebrafish larvae. Biotech. Histochem. *82*, 23–28.
45. Hilpelä, P., Vartiainen, M.K., and Lappalainen, P. (2004). Regulation of the Actin Cytoskeleton by PI(4,5)P2 and PI(3,4,5)P3. In Current Topics in Microbiology and Immunology (Springer), pp. 117–163.
46. Yin, H.L., and Janmey, P.A. (2003). Phosphoinositide Regulation of the Actin Cytoskeleton. Annu. Rev. Physiol. *65*, 761–789.
47. Rozelle, A.L., Machesky, L.M., Yamamoto, M., Driessens, M.H., Insall, R.H., Roth, M.G., Luby-Phelps, K., Marriott, G., Hall, A., and Yin, H.L. (2000). Phosphatidylinositol 4,5-bisphosphate induces actin-based movement of raft-enriched vesicles through WASP-Arp2/3. Curr. Biol. *10*, 311–320.
48. van Horck, F.P.G., Lavazais, E., Eickholt, B.J., Moolenaar, W.H., and Divecha, N. (2002). Essential Role of Type Iα Phosphatidylinositol 4-Phosphate 5-Kinase in Neurite Remodeling. Curr. Biol. *12*, 241–245.
49. Kisseleva, M., Feng, Y., Ward, M., Song, C., Anderson, R.A., and Longmore, G.D. (2005). The LIM Protein Ajuba Regulates Phosphatidylinositol 4,5-Bisphosphate Levels in Migrating Cells through an Interaction with and Activation of PIPKIα. Mol. Cell Biol. *25*, 3956–3966.
50. Yarar, D., Waterman-Storer, C.M., and Schmid, S.L. (2005). A Dynamic Actin Cytoskeleton Functions at Multiple Stages of Clathrin-mediated Endocytosis. Mol. Biol. Cell *16*, 964–975.
51. Puthenveedu, M.A., Lauffer, B., Temkin, P., Vistein, R., Carlton, P., Thorn, K., Taunton, J., Weiner, O.D., Parton, R.G.,

and von Zastrow, M. (2010). Sequence-Dependent Sorting of Recycling Proteins by Actin-Stabilized Endosomal Microdomains. Cell *143*, 761–773.

52. Mayle, K.M., Le, A.M., and Kamei, D.T. (2012). The intracellular trafficking pathway of transferrin. Biochim. Biophys. Acta *1820*, 264–281.
53. Gammella, E., Buratti, P., Cairo, G., and Recalcati, S. (2017). The transferrin receptor: the cellular iron gate. Metallomics *9*, 1367–1375.
54. Rosello, M., Vougny, J., Czarny, F., Mione, M.C., Concordet, J.-P., Albadri, S., and del Bene, F. (2021). Precise base editing for the in vivo study of developmental signaling and human pathologies in zebrafish. Elife *10*, e65552.
55. Mirzaa, G.M., Conway, R.L., Gripp, K.W., Lerman-Sagie, T., Siegel, D.H., DeVries, L.S., Lev, D., Kramer, N., Hopkins, E., Graham, J.M., and Dobyns, W.B. (2012). Megalencephaly-capillary malformation (MCAP) and megalencephaly-polydactyly-polymicrogyria-hydrocephalus (MPPH) syndromes: Two closely related disorders of brain overgrowth and abnormal brain and body morphogenesis. Am. J. Med. Genet. *158A*, 269–291.
56. Mirzaa, G.M., Conti, V., Timms, A.E., Smyser, C.D., Ahmed, S., Carter, M., Barnett, S., Hufnagel, R.B., Goldstein, A., Narumi-Kishimoto, Y., et al. (2015). Characterisation of mutations of the phosphoinositide-3-kinase regulatory subunit, PIK3R2, in perisylvian polymicrogyria: a next-generation sequencing study. Lancet Neurol. *14*, 1182–1195.
57. Baulac, S., Lenk, G.M., Dufresnois, B., Ouled Amar Bencheikh, B., Couarch, P., Renard, J., Larson, P.A., Ferguson, C.J., Noé, E., Poirier, K., et al. (2014). Role of the phosphoinositide phosphatase FIG4 gene in familial epilepsy with polymicrogyria. Neurology *82*, 1068–1075.
58. Frazier, T.W., Embacher, R., Tilot, A.K., Koenig, K., Mester, J., and Eng, C. (2015). Molecular and phenotypic abnormalities in individuals with germline heterozygous PTEN mutations and autism. Mol. Psychiatry *20*, 1132–1138.
59. Gerasimavicius, L., Livesey, B.J., and Marsh, J.A. (2022). Loss-of-function, gain-of-function and dominant-negative mutations have profoundly different effects on protein structure. Nat. Commun. *13*, 3895. https://doi.org/10.1038/s41467-022-31686-6.
60. Allen, P.G. (2003). Actin filament uncapping localizes to ruffling lamellae and rocketing vesicles. Nat. Cell Biol. *5*, 972–979.
61. Cui, S., Guerriero, C.J., Szalinski, C.M., Kinlough, C.L., Hughey, R.P., and Weisz, O.A. (2010). OCRL1 function in renal epithelial membrane traffic. Am. J. Physiol. Renal Physiol. *298*. F335–F345.
62. ben El Kadhi, K., Roubinet, C., Solinet, S., Emery, G., and Carréno, S. (2011). The Inositol 5-Phosphatase dOCRL Controls PI(4,5)P2 Homeostasis and Is Necessary for Cytokinesis. Curr. Biol. *21*, 1074–1079.
63. Oude Weernink, P.A., Schmidt, M., and Jakobs, K.H. (2004). Regulation and cellular roles of phosphoinositide 5-kinases. Eur. J. Pharmacol. *500*, 87–99.
64. Shibasaki, Y., Ishihara, H., Kizuki, N., Asano, T., Oka, Y., and Yazaki, Y. (1997). Massive Actin Polymerization Induced by Phosphatidylinositol-4-phosphate 5-Kinase in Vivo. J. Biol. Chem. *272*, 7578–7581.
65. Gervais, L., Claret, S., Januschke, J., Roth, S., and Guichet, A. (2008). PIP5K-dependent production of PIP2 sustains microtubule organization to establish polarized transport in the Drosophila oocyte. Development *135*, 3829–3838.
66. Weernink, P.A.O., Meletiadis, K., Hommeltenberg, S., Hinz, M., Ishihara, H., Schmidt, M., and Jakobs, K.H. (2004). Activation of Type I Phosphatidylinositol 4-Phosphate 5-Kinase Isoforms by the Rho GTPases, RhoA, Rac1, and Cdc42. J. Biol. Chem. *279*, 7840–7849.
67. Cajigas, I.J., Will, T., and Schuman, E.M. (2010). Protein homeostasis and synaptic plasticity. EMBO J. *29*, 2746–2752.
68. Wenk, M.R., Pellegrini, L., Klenchin, V.A., Di Paolo, G., Chang, S., Daniell, L., Arioka, M., Martin, T.F., and De Camilli, P. (2001). PIP Kinase Iγ Is the Major PI(4,5)P2 Synthesizing Enzyme at the Synapse. Neuron *32*, 79–88. https://doi.org/10.1016/S0896-6273(01)00456-1.
69. Wang, Y., Lian, L., Golden, J.A., Morrisey, E.E., and Abrams, C.S. (2007). PIP5KIγ is required for cardiovascular and neuronal development. Proc. Natl. Acad. Sci. USA *104*, 11748–11753.
70. Ulicna, L., Kalendova, A., Kalasova, I., Vacik, T., and Hozák, P. (2018). PIP2 epigenetically represses rRNA genes transcription interacting with PHF8. Biochim. Biophys. Acta. Mol. Cell Biol. Lipids *1863*, 266–275.
71. Qi, H.H., Sarkissian, M., Hu, G.-Q., Wang, Z., Bhattacharjee, A., Gordon, D.B., Gonzales, M., Lan, F., Ongusaha, P.P., Huarte, M., et al. (2010). Histone H4K20/H3K9 demethylase PHF8 regulates zebrafish brain and craniofacial development. Nature *466*, 503–507.
72. Laumonnier, F., Holbert, S., Ronce, N., Faravelli, F., Lenzner, S., Schwartz, C.E., Lespinasse, J., Van Esch, H., Lacombe, D., Goizet, C., et al. (2005). Mutations in PHF8 are associated with X linked mental retardation and cleft lip/cleft palate. J. Med. Genet. *42*, 780–786.
73. Maffucci, T., Raimondi, C., Abu-Hayyeh, S., Dominguez, V., Sala, G., Zachary, I., and Falasca, M. (2009). A Phosphoinositide 3-Kinase/Phospholipase Cgamma1 Pathway Regulates Fibroblast Growth Factor-Induced Capillary Tube Formation. PLoS One *4*, e8285.
74. Hatch, N.E. (2010). FGF Signaling in Craniofacial Biological Control and Pathological Craniofacial Development. Crit. Rev. Eukaryot. Gene Expr. *20*, 295–311.
75. Schurmans, S., Vande Catsyne, C.-A., Desmet, C., and Moës, B. (2021). The phosphoinositide 5-phosphatase INPP5K: From gene structure to in vivo functions. Adv. Biol. Regul. *79*, 100760.
76. D'Amico, A., Fattori, F., Nicita, F., Barresi, S., Tasca, G., Verardo, M., Pizzi, S., Moroni, I., De Mitri, F., Frongia, A., et al. (2020). A Recurrent Pathogenic Variant of INPP5K Underlies Autosomal Recessive Congenital Muscular Dystrophy With Cataracts and Intellectual Disability: Evidence for a Founder Effect in Southern Italy. Front. Genet. *11*, 565868.
77. Wright, B.D., Loo, L., Street, S.E., Ma, A., Taylor-Blake, B., Stashko, M.A., Jin, J., Janzen, W.P., Frye, S.v., and Zylka, M.J. (2014). The lipid kinase PIP5K1C regulates pain signaling and sensitization. Neuron *82*, 836–847.